Inorganic Chemistry

Article

Isomerization Mechanisms of Stereolabile *tris*- and *bis*-Bidentate Octahedral Cobalt(II) Complexes: X-ray Structure and Variable Temperature and Pressure NMR Kinetic Investigations

Fabrice Riblet,[‡] Ghenadie Novitchi,*[†,‡] Rosario Scopelliti,[‡] Lothar Helm,*[‡] Aurelian Gulea,[§] and André E. Merbach*[‡]

[†]*Institute of Chemistry, Academy of Sciences of Moldova, Academiei str. 3. MD-2028 Chisinau, Moldova,* [‡]*Laboratoire de Chimie Inorganique et Bioinorganique, Ecole Polytechnique Fédérale de Lausanne, CH-1015, Lausanne, Switzerland, and* [§]*Department of Chemistry Moldova State University, A. Mateevici str. 60, MD-2009 Chisinau, Moldova*

The isomerization dynamics of five labile octahedral Co(II) compounds have been investigated by variable temperature and pressure ^{1}H and ^{19}F NMR spectroscopy in dichloromethane solution. The X-ray crystal structure of the two *tris*-chelates, [Co(HFA)$_2$bpic] (**1**) and [Co(TTFA)$_2$bpy] (**2**), show a distorted octahedral arrangement of the 4 oxygen and 2 nitrogen donor atoms, with bidentate ligand bite angles smaller than 90°. On the other hand, in the three *bis*-chelates, *trans*(N)-[Co(HFA)$_2$(CH$_3$py)$_2$](**3**), *cis*(N)-*cis*(CF$_3$)-*trans*(S)-[Co(TTFA)$_2$(CH$_3$py)$_2$](**4**), and *trans*(N)-*trans*(CF$_3$)-[Co(TTFA)$_2$(CF$_3$py)$_2$](**5**), the replacement of the bidentate nitrogen donor ligands by two monodentate Rpy ligands leads to relaxed structures with almost regular octahedral arrangements of the donor atoms (HFA = 1,1,1,5,5,5-hexafluoro-2,4-pentanedionato anion; TTFA = 4,4,4-trifluoro-1-(2-thienyl)-1,3-butanedionato anion; bpy = 2,2′-bipyridine; bpic = 4,4′-dimethyl-2,2′-bipyridine). In solution the five complexes are stereolabile and all possible isomers are formed: from one for **1** up to five for **4** and **5**. All *cis*-N isomers form pairs of enantiomers, whereas the *trans*-N isomers are achiral. A solid state structure/isomerization mechanism/rate correlation has been established for the isomerization dynamics of these Co(II) *tris*- and *bis*-chelates. The two *tris*-chelate complexes **1** and **2**, with a distorted octahedral solid state structure, show one and three isomers in solution and isomerize/tautomerize very rapidly according to Bailar twist mechanisms. The three *bis*-chelate complexes **3**, **4**, and **5**, with a close to octahedral symmetry in the solid state, show two, five, and five isomers, respectively. They isomerize/tautomerize 3 orders of magnitude slower as the *tris*-chelates, by an intramolecular dissociative mechanism involving a ring-opening of an arm of a bidentate ligand to form a TBP intermediate with a dangling bidentate ligand. The results of this first systematic investigation of the isomerization mechanisms of highly labile Co(II) complexes are supported by the NMR observed exchange paths (up to five for complexes for **4** and **5**), the variable temperature (185 to 312 K) and pressure (up to 200 MPa) activation parameters, and a detailed analysis of the solid state structures.

1. Introduction

Since the early Werner time of coordination chemistry many mechanistic studies have been carried out on slow geometric isomerization and racemization reactions of complexes. These kinetically slow processes with half-lives of minutes or longer were usually monitored by spectrophotometry or polarimetry, including chromatography.[1] The study of the stereochemical non-rigidity of metal−ligand complexes has changed dramatically in the 1960s with the development of NMR techniques. Not only do they provide a means of assigning structures in solution, but they allow determining equilibrium constants, exchange rates, and reaction pathways between isomers. What was already feasible with other techniques for slow reactions became also possible for highly

To whom correspondence should be addressed. E-mail: ghenadie. novitchi@googlemail.com (G.N.); lothar.helm@epfl.ch (L.H.); andre. merbach@epfl.ch (A.M.). Phone: +373 22 73 97 81 (G.N.); +41 21 693 98 75 (L.H.); +41 21 693 98 71 (A.M.).

(1) Basolo, F.; Pearson, R. G. *Mechanisms of Inorganic Reactions*, 2nd ed.; John Wiley and Sons, Inc.: New York, 1967.

(2) Serpone, N.; Bickley, D. G. *Prog. Inorg. Chem.* **1972**, *17*, 391–566.

(3) Holm, R. H.; Hawkins, C. J. Stereochemistry and Structural and Electronic Equilibria. In *NMR of Paramagnetic Molecules*; La Mar, G. N., Horrocks, W. D., Holm, R. H., Eds.; Academic Press: New York, 1973; pp 243−331.

labile coordination compounds.[2−5] Isomerization reactions of six-coordinate complexes of trivalent (Al,[6] Ga,[6,7] Sc,[8] Co, Rh, Ru, V,[9] Mn, Fe, Cr) and tetravalent (Pt, Ti,[10] Zr, Hf, Ge, Sn) metal ions with three or two bidentate chelates L have been extensively studied experimentally. More recently experimental studies have been complemented by theoretical calculations.[9−15] Quantitative kinetic studies of isomerization of similar chelates of 3d divalent ions are scarce. They deal with Fe[II], Ni[II], and early Co[II] studies of a *tris*-chelate [Co(acac)$_2$(4,7-dimethyl-1,10-phenantroline)][16] and of *bis*-chelates: [Co(acac)$_2$(Rpy)$_2$] (R = H,[17] CH$_3$[18]) and [Co(O$_2$-CR)$_2$(Rpy)$_2$].[19]

The possible isomerization and racemization mechanisms and their idealized transition states are best introduced with the simplest representative complexes: the *tris*-chelated metal complexes ML$_3$ with a symmetrical bidentate chelant L. They exist as Δ and Λ isomers, and can racemize according to mechanisms described in Figure 1.[1] Non-bond rupture twist mechanisms are operative in the majority of cases. In the case of the Bailar twist, the rotation takes place around the C_3 axis of the idealized D_3 point group symmetry of the octahedral structure. As a consequence, the trigonal prismatic transient shows a structure with three parallel chelants. In the case of the Rây−Dutt twist the rotation takes place around a pseudo-C_3 axis of the complex (a C_3 axis of the octahedron defined by the donor atoms of the complex which is not a C_2 axis of the D_3 ML$_3$ complex) to generate a C_{2v} symmetric transient. More rarely the racemization can start with the breaking of one metal-donor bond and continue with an internal rearrangement of the resulting five-coordinated intermediate. These dissociative paths can be classified as square-pyramid paths (SP-paths) and trigonal-bipyramid paths with equatorial or axial dangling ligand (TPB-paths) according to the transient structure. For less symmetrical complexes (mixed bidentate, monodentate ligands), the possible reaction paths between isomers are often summarized in topological diagrams.[2] Some paths may interconvert geometrical isomers or not, and result or not in simultaneous optical inversion. Detailed comparison of NMR kinetics results with various rearrangements paths
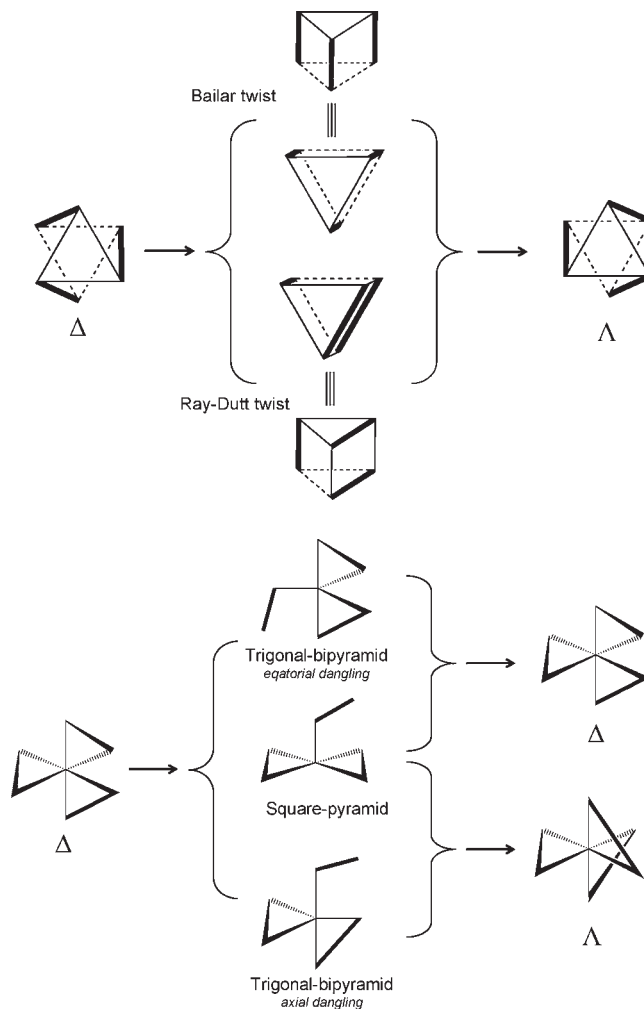
Figure 1. Representation of reaction paths normally postulated for intramolecular isomerization of *tris*-chelate complexes with symmetric ligands.

can lead to the assignment of the most probable mechanism characterized by its topological diagram.

Cobalt(II) six-coordinate *tris*- and *bis*-chelates are of interest in the field of coordination chemistry as structural prototypes to investigate the isomerization mechanisms. They demonstrate the capability to exist in solution as a large number of isomers in fast isomeric and enantiomeric equilibria detectable by NMR. In two preliminary reports we have shown the richness of their structural isomerism[20] and the strength of the NMR line-broadening technique to assign the interconversion mechanism[21] between the five labile isomers of [Co(TTFA)$_2$(CH$_3$py)$_2$]. In this paper we start with a simple [Co(A-A)$_2$(C-C)] *tris*-chelate with mixed symmetrical bidentate ligands and increase progressively the complexity, for example, the number of isomers, and finish with *bis* asymmetrical bidentate ligand − *bis* monodentate ligand [Co(A-B)$_2$c$_2$] complexes (Figure 2). Throughout the series of complexes studied all possible isomers are observed in CD$_2$Cl$_2$ solution. The kinetic parameters governing their enantiomerization and isomerization will be discussed, in particular with respect to the X-ray structures from the isolated complexes.

(4) Pignolet, L. H.; La Mar, G. N. Dynamics of Intramolecular Rearrangements. In *NMR of Paramagnetic Molecules*; La Mar, G. N., Horrocks, W. D., Holm, R. H., Eds.; Academic Press: New York, 1973; pp 333−369.

(5) Pignolet, L. H. *Top. Curr. Chem.* **1975**, *56*, 91−137.

(6) Kite, K.; Orrell, K. G.; Sik, V.; Roger, Y. *Polyhedron* **1995**, *14*, 2711−2722.

(7) Gromova, M.; Jarjayes, O.; Hamman, S.; Nardin, R.; Beguin, C.; Willem, R. *Eur. J. Inorg. Chem.* **2000**, 545−550.

(8) Hatakeyama, Y.; Kido, H.; Harada, M.; Tomiyasu, H.; Fukutomi, H. *Inorg. Chem.* **1988**, *27*, 992−996.

(9) Rikkou, M.; Manos, M.; Tolis, E.; Sigalas, M. P.; Kabanos, T. A.; Keramidas, A. D. *Inorg. Chem.* **2003**, *42*, 4640−4649.

(10) Davis, A. V.; Firman, T. K.; Hay, B. P.; Raymond, K. N. *J. Am. Chem. Soc.* **2006**, *128*, 9484−9496.

(11) Amati, M.; Lelj, F. *Chem. Phys. Lett.* **2002**, *363*, 451−457.

(12) Montgomery, C. G.; Shorrock, C. J. *Inorg. Chim. Acta* **2002**, *328*, 259−262.

(13) Rzepa, H. S.; Cass, M. E. *Inorg. Chem.* **2007**, *46*, 10444.

(14) Rzepa, H. S.; Cass, M. E. *Inorg. Chem.* **2007**, *46*, 8024−8031.

(15) Amati, M.; Lelj, F. *Theor. Chem. Acc.* **2008**, *120*, 447−457.

(16) La Mar, G. N. *J. Am. Chem. Soc.* **1970**, *92*, 1806−1807.

(17) Lincoln, S. F. *J. Chem. Soc., Dalton Trans.* **1973**, 1896−1899.

(18) Kluiber, R. W.; Kukla, R.; Horrocks, W. D. *Inorg. Chem.* **1970**, *9*, 1319−1325.

(19) Goodacre, A.; Orrell, K. G. *J. Chem. Soc., Dalton Trans.* **1983**, 153−159.

(20) Novitchi, G.; Riblet, F.; Helm, L.; Scopelliti, R.; Gulea, A.; Merbach, A. E. *Magn. Reson. Chem.* **2004**, *42*, 801−806.

(21) Riblet, F.; Novitchi, G.; Helm, L.; Gulea, A.; Merbach, A. E. *Chimia* **2006**, *60*, 224−227.
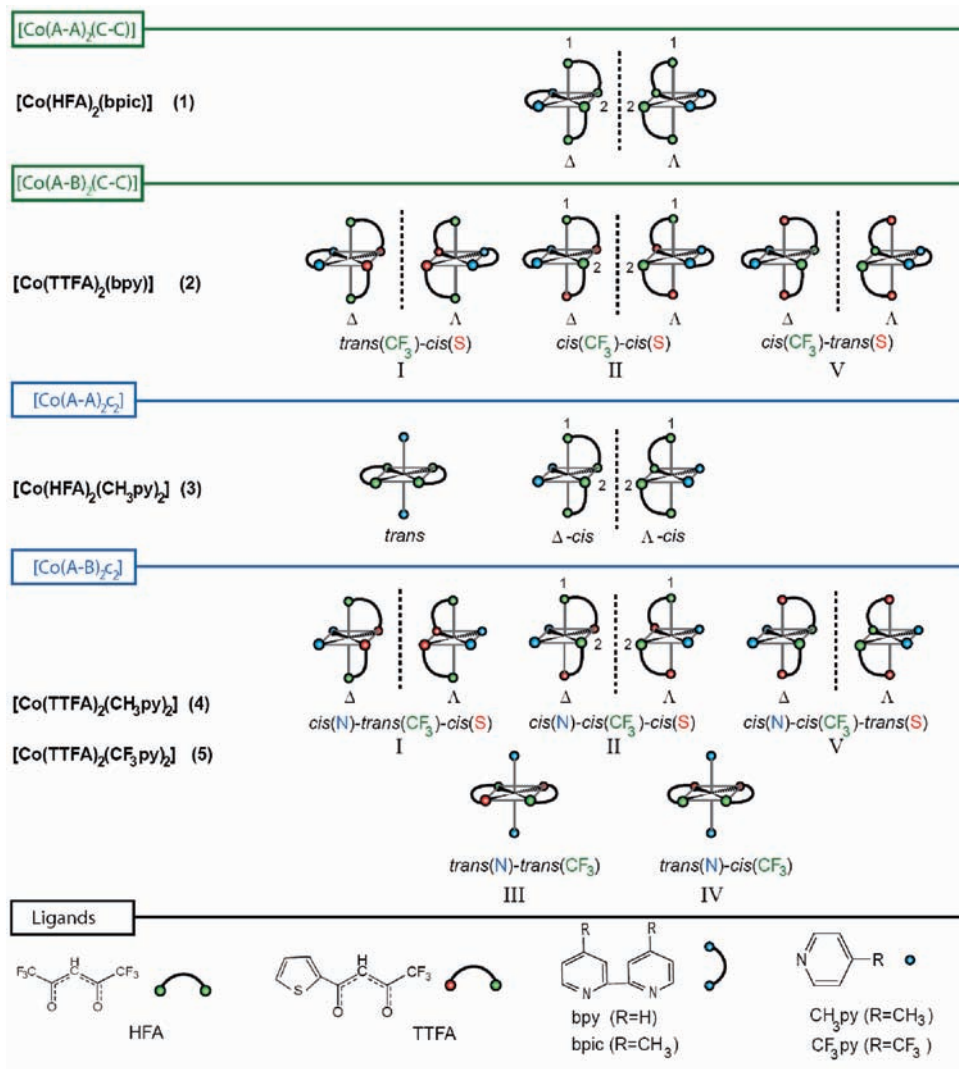
Figure 2. Structure and isomers of five cobalt(II) *tris-* and *bis-*bidentate complexes with the general formula [Co(A-A)₂(C-C)], [Co(A-B)₂(C-C)], [Co(A-A)₂c₂], and [Co(A-B)₂c₂].

2. Experimental Section

2.1. Chemicals. Starting materials and solvents used were purchased from Aldrich. Deuterated solvents CD₂Cl₂, CD-Cl₃ (99.8%), toluene-d₈ (99.5%) were obtained from Aldrich, Dr Glaser, and AR MAR, respectively. These chemicals were used without further purification.

2.2. Synthesis. [Co(HFA)₂(H₂O)₂] (HFA = 1,1,1,5,5,5-hexa-fluoro-2,4-pentanedionato anion) and [Co(TTFA)₂(H₂O)₂] (TTFA = 4,4,4-trifluoro-1-(2-thienyl)-1,3-butanedionato anion) were prepared according to literature procedure[20] and recrystallized from methanol. The amine complexes **1–5** (Figure 2) were obtained by dissolving the aqua complexes in hot ethanol containing a stoichiometric amount of the amine (bpy = 2,2′-bipyridine, bpic = 4,4′-dimethyl-2,2′-bipyridine, CH₃py, CF₃py). The solutions were cooled, and the resulting products filtered and washed with a minimum of cold ethanol (elemental analyses are given in the Supporting Information, Table S1).[20]

2.3. X-ray Crystal Measurements. Data collections for the five crystal structures were performed at low temperature (the structure of **4** at room temperature (RT) has been reported previously[22]) using Mo Kα radiation. An Oxford Diffraction

Sapphire/KM4 CCD was employed for **1**, **2**, and **3** while the remaining samples were measured on a Bruker APEX II CCD. Both diffractometers have a kappa geometry goniometer. Data were reduced by means of CrysAlisPro[23] (**1**, **2**, **3**), and EvalCCD[24] (**4**, **5**) and then corrected for absorption.[25] Solution and refinement for all crystal structures were performed by SHELXTL.[26] All structures were refined using full-matrix least-squares on F^2 with all non hydrogen atoms anisotropically defined. Hydrogen atoms were placed in calculated positions by means of the "riding" model. All structures having a thienyl moiety (**2**, **4**, **5**) show a disorder problem because of the free rotation along the single C−C bond; this was solved by means of the split model and then fixing the C−S and C=C bonds within the heterocyclic ring. Twinning problems were discovered in the case of **1**. The twinning by reticular mero-hedry was analyzed by the TWINROTMAT routine of PLA-TON.[27] A HKLF5 file was then generated and used in the

(22) Pretorius, J. A.; Boeyens, J. C. A. *J. Inorg. Nucl. Chem.* **1978**, *40*, 407–416.

(23) *CrysAlisPro*; Oxford Diffraction Ltd.: Abingdon, Oxfordshire, U.K., 2008.

(24) Duisenberg, A. J. M.; Kroon-Batenburg, L. M. J.; Schreurs, A. M. M. *J. Appl. Crystallogr.* **2003**, *36*, 220–229.

(25) Blessing, R. H. *Acta Crystallogr., Sect. A* **1995**, 51.

(26) *SHELXTL*, 6.1.4.; Bruker AXS Inc.: Madison, WI, 2003.

(27) Spek, A. L. *J. Appl. Crystallogr.* **2003**, *36*, 7–13.

Table 1. Crystal Data and Details of the Structure Determination for Compounds **1**−**5**

	1	**2**	**3**	**4**	**5·C₆H₅CH₃**
solvent recryst.	MeOH	CH_2Cl_2	MeOH	CH_2Cl_2	$C_6H_5CH_3$
chemical formula	$C_{22}H_{14}CoF_{12}N_2O_4$	$C_{26}H_{16}CoF_6N_2O_4S_2$	$C_{22}H_{16}CoF_{12}N_2O_4$	$C_{28}H_{22}CoF_6N_2O_4S_2$	$C_{35}H_{24}CoF_{12}N_2O_4S_2$
formula weight	657.28	657.46	659.30	687.53	887.61
crystal system	monoclinic	triclinic	orthorhombic	monoclinic	triclinic
space group	$P2_1/n$	$P\bar{1}$	$Cmcm$	$C2/c$	$P\bar{1}$
a (Å)	8.5612(5)	7.9907(4)	9.6976(9)	9.3586(19)	9.337(2)
b (Å)	16.6911(7)	10.9673(7)	16.3685(15)	17.725(4)	9.6786(12)
c (Å)	18.4723(8)	15.2687(10)	15.9331(18)	17.852(4)	11.5297(17)
α (deg)	90	85.318(5)	90	90	96.473(14)
β (deg)	101.772(5)	86.455(5)	90	94.12(3)	101.131(15)
γ (deg)	90	85.810(5)	90	90	110.333(19)
vol (Å³)	2584.1(2)	1327.96(14)	2529.1(4)	2953.7(10)	940.2(3)
Z	4	2	4	4	1
D_{calc} (g cm⁻³)	1.689	1.644	1.731	1.546	1.568
$F(000)$	1308	662	1316	1396	447
μ (mm⁻¹)	0.783	0.883	0.800	0.797	0.668
temp (K)	140(2)	140(2)	140(2)	100(2)	100(2)
wavelength (Å)	0.71073	0.71073	0.71073	0.71073	0.71073
measured reflections	4185	8461	7626	9970	19364
unique reflections	4185	4141	1235	2547	4264
unique reflections $[I > 2\sigma(I)]$	3052	2188	1069	1479	3360
data/parameters	4185/371	4141/392	1235/113	2547/204	4264/266
R^a $[I > 2\sigma(I)]$	0.0535	0.0447	0.0312	0.0756	0.0575
$wR2^a$ (all data)	0.1419	0.0736	0.0770	0.1358	0.1465
GoF^b	1.113	0.828	1.081	1.094	1.097

$^a R = \sum||F_o| - |F_c||/\sum|F_o|$, $wR2 = \{\sum w(F_o{}^2 - F_c{}^2)^2/\sum w(F_o{}^2)^2\}^{1/2}$. $^b \mathrm{GoF} = \{\sum[w(F_o{}^2 - F_c{}^2)^2]/(n-p)\}^{1/2}$ where n is the number of data and p is the number of parameters refined.

refinement of the structure, obtaining a final BASF parameter of 0.115(6).

2.4. NMR Measurements. All samples were prepared in N_2 atmosphere by weighing complexes and excess ligand in 5 mm NMR tubes and adding 0.5 mL of CD_2Cl_2. The concentrations of the complexes were about 10 mM. The ^1H chemical shifts were referred to TMS using the residual signals from the solvent CD_2Cl_2 (5.32 ppm) and the ^{19}F chemical shift to internal $CFCl_3$ (+78.5 ppm) or external CF_3COOH (0 ppm). For kinetics the NMR frequencies are referred to an arbitrary spectrometer frequency. The ^1H and ^{19}F NMR spectra were recorded on a Bruker DRX-400 spectrometer (9.4 T, resonance frequencies: 400.2 and 376.5 MHz, respectively). Typical spectral conditions for ^1H and ^{19}F NMR were 8k data points for the time domain, the spectrum window was up to 70 kHz, and the number of scans chosen was 32 and 512. The temperature was controlled within ±0.1 K using a Bruker BVT 3000 unit and was measured before or after spectral acquisition using a substitution method.[28] High-pressure high resolution spectra were monitored with a home-built narrow bore probe (5 mm NMR tube).[29]

2.5. NMR Data Analyses. In the slow exchange NMR approximation the line widths and integrals of NMR signals were obtained by fitting Lorentzian functions to the experimental spectra using the NMRICMA[30] program for MATLAB. The adjustable parameters are the resonance frequency, intensity, line width, baseline, and phasing. The thermodynamic parameters for the isomerization reactions (eq 1) are obtained from the mole fractions P_j of the different isomers. The ratios of the mole fractions of the isomers (P_j/P_r) are equal to the corresponding relative stability constants $K_{r,j}$, were r stands for the isomer used as a reference. The mole fractions are related to the variable temperature and pressure thermodynamic parameters

through eqs 2 and 3, with $i \neq r$.

$$\text{isomer-}r \leftrightarrow \text{isomer-}j \tag{1}$$
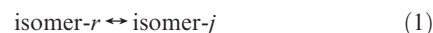
$$P_j = (1 - \sum P_i) \exp(\Delta S^{\circ}_{r,j}/R - \Delta H^{\circ}_{r,j}/RT) \tag{2}$$

$$P_j = (1 - \sum P_i) \exp(-\Delta V^{\circ}_{r,j}/RT) \tag{3}$$

In the variable temperature and pressure kinetic analysis the total number of isomerization rate constants could be divided by two by taking into account the equilibrium constants linking forward and backward isomerization reactions. The transverse relaxation rates $1/T_2{}^j$ are related to the activation parameters‡ through eqs 4 to 8.

$$1/T_2{}^j = \sum k_{j>i} + 1/T_2{}^{para,j} \tag{4}$$

$$k_{j>i}(T) = k_B T/h \exp(\Delta S^{\ddagger}_{j>i}/R - \Delta H^{\ddagger}_{j>i}/RT) \tag{5}$$

$$k_{j>i}(P) = k_{j>i}(P_0) \exp(-\Delta V^{\ddagger}_{j>i}P/RT) \tag{6}$$

$$1/T_2{}^{para,j}(T) = 1/T_2{}^{para,j}(T_0) \exp[E_{a,j}/R(1/T - 1/T_0)] \tag{7}$$

$$1/T_2{}^{para,j}(P) = 1/T_2{}^{para,j}(P_0) \exp(-\Delta V^{\ddagger}_{para,j}P/RT) \tag{8}$$

In the slow NMR exchange regime the eqs 2, 4, 5 and 7 were used to fit simultaneously the populations P_j and the transverse relaxation rates $1/T_2{}^j$, to obtain the variable temperature equilibrium and kinetic parameters (eqs 3, 4, 6 and 8 for variable pressure).

In the fast exchange regime complete line-shape analyses based on the Kubo−Sack formalism[31] using modified Bloch equations were performed with NMRICMA to extract the rate constants from the experimental spectra. Each spectrum was

(28) Ammann, C.; Meier, P.; Merbach, A. E. *J. Magn. Reson.* **1982**, *46*, 319–321.

(29) Cusanelli, A.; Nicula-Dasci, L.; Frey, U.; Merbach, A. E. *Inorg. Chem.* **1997**, *36*, 2211–2217.

(30) Helm, L. *NMRICMA*, 3.1.5; EPFL: Lausanne, Switzerland, 2003.

(31) Johnson, C. S.; Moreland, C. *J. Chem. Educ.* **1973**, *50*, 477–483.
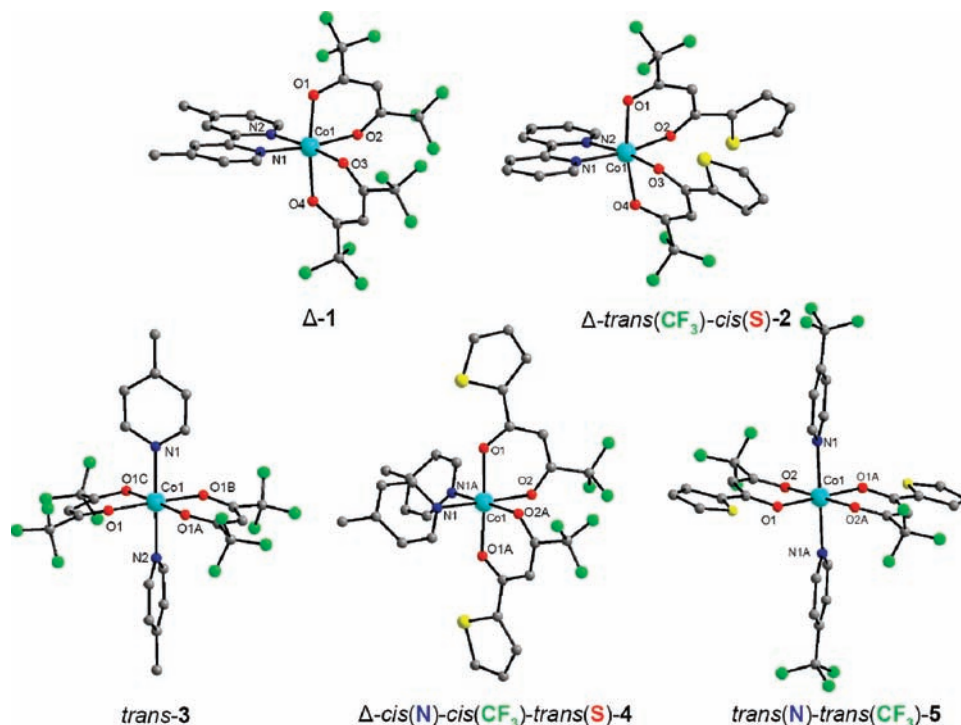
Figure 3. Molecular structure of the **1**−**5** Co(II) complexes.

analyzed separately using an appropriate exchange matrix for each isomerization mechanism. Best extrapolated values from low temperature data are used for the resonance frequency (linear with $1/T$), the intensity, and the mono exponential paramagnetic contribution to the transverse relaxation rate. To improve the phasing of the fitting, both the real and imaginary parts of the spectra were treated simultaneously (Supporting Information, Figure S1). The resulting data are then analyzed simultaneously with eqs 2 and 5 (or 6) for variable temperature (or pressure) series of experiments. Data analysis was carried out with the nonlinear least-squares fitting program VISUALIZEUR-OPTIMISEUR[32] for MATLAB, using the Levenberg−Marquardt algorithm.

3. Results

3.1. Solid State Structures. The structures of complexes **1** to **5** were determined by X-ray crystallography. The crystallographic data are presented in Table 1 and the structures shown in Figure 3. Selected bond lengths and angles of **1** to **5** and of similar compounds are listed in Table 2.

The compound [Co(HFA)$_2$bpic] (**1**), belonging to the [Co(A-A)$_2$(C-C)] type (Figure 2), contains two bidentate 1,1,1,5,5,5-hexafluoro-2,4-pentanedionato ligands and one bidentate 4,4′-dimethyl-bipyridine ligand (Figure 3). The unit cell is made of two Δ-**1** and two Λ-**1** enantiomers. The cobalt atom is in a distorted octahedral environment with bidentate ligand bite angles smaller than 90° (for O−Co−O: 86.81(14)° and 86.57(13)°; for N−Co−N: 78.07(15)° only), and with a non-linearity of the O1−Co−O4 angle: 172.04(13)°. The Co−O bonds (2.065(3), 2.068(3), 2.069(3) and 2.081(3) Å) are longer than those observed in [Co(HFA)$_2$(CH$_3$py)$_2$] (**3**) (2.060(1) Å). Both enantiomers of **1** are involved in $\pi-\pi$ staking and form

the crystal packing of compound **1** (Supporting Information, Figure S2).

The second cobalt *tris*-chelate [Co(TTFA)$_2$bpy] (**2**), belonging to the [Co(A-B)$_2$(C-C)] type, contains two asymmetric bidentate 4,4,4-trifluoro-1-(2-thienyl)-1,3-butanedionato ligands and similarly to **1** one symmetrical bidentate bipyridine type ligand (Figure 3). In this case three different pairs of enantiomers are possible (Figure 2). The recrystallization of **2** in dichloromethane produces crystals (I-**2**) with one Δ- and one Λ-*trans*(CF$_3$) enantiomer per unit cell. Again Co is in a distorted octahedral environment with even slightly smaller ligand bite angles (for O−Co−O: 86.05(11)° and 85.75(12)°; for N−Co−N: 77.59(14)°) and an increased non-linearity of the O1−Co−O4 angle (169.07(11)°) compared to compound **1**. The distortion from octahedral symmetry is also reflected for both **1** and I-**2** by the large values of their O1−Co−N2 and O4−Co−N1 angles (between 96.67(15)° and 99.92(12)°). In both compounds the Co−N1 and Co−N2 distances are the same within experimental errors, but they are slightly shorter for **1** (average 2.087 Å) than for I-**2** (average 2.097 Å). A difference is observed in I-**2** between the Co−O1/4(CF$_3$) (average 2.067 Å) and the Co−O2/3(thienyl) (average 2.051 Å) bond lengths. In other words the corresponding Co−O(CF$_3$) weaker bond strength because of the electro-attractive CF$_3$ is compensated by an increase in the Co−O(thienyl) bond strength. Finally the crystal packing in I-**2** also involves specific $\pi-\pi$ staking of the aromatic rings of the bpy ligands. The replacement of the bipyridine type of ligands by ethylendiamine type of ligands results in an increase of the bite angles of the ligands with average values of 87.4°, 87.18°, 87.21°, and 87.2° for the OCoO bites and 82.3°, 82.20°, 82.6°, and 81.7° for the NCoN bites in [Co(ac)$_2$(Me$_4$en)],[38] [Co(ac)$_2$(Et$_4$en)],[33,42] [Co(TTFA)$_2$(Me$_4$en)],[34] and [Co(TTFA)$_2$(Me$_2$en)],[34] respectively (Table 2). This angle increase

(32) Yerly, F. *VISUALISEUR*; EPFL: Lausanne, Switzerland, 2001.

Table 2. Selected Bond Lengths and Angles for **1** to **5** and Similar *cis*- and *trans*-Co(II) Chelates[a,b]

cis(N)-Complexes

		sym.	Co–O1	Co–O2	Co–O3	Co–O4	Co–N1	Co–N2	O1CoO2	O3CoO4	N1CoN2	O1CoO4	O1CoN1	O1CoN2	O4CoN1	O4CoN2
Co(A-A)₂(C-C)	[Co(HFA)₂bpic] (**1**)	C_1	2.065(3)	2.068(3)	2.069(3)	2.081(3)	2.085(4)	2.090(4)	86.81(14)	86.57(13)	78.07(15)	172.04(13)	86.95(15)	96.86(15)	96.67(15)	90.83(14)
	[Co(ac)₂(Me₄en)][c]	C_1	2.043	2.076	2.090	2.046	2.237	2.218	88.1	86.7	82.3	175.2	89.3	94.9	94.9	88.0
	[Co(ac)₂(Et₄en)][d,e]	C_2	2.037	2.071	2.071#	2.037#	2.262	2.262#	87.18	87.18#	82.20	178.70	90.39	90.58	90.58#	90.39#
Co(A-B)₂(C-C)	[Co(TTFA)₂bpy] (**2**)	C_1	2.068(3)	2.051(3)	2.051(2)	2.065(3)	2.098(3)	2.096(3)	86.05(11)	85.75(12)	77.59(11)	169.07(13)	88.63(12)	98.69(12)	99.92(12)	89.85(12)
	[Co(TTFA)₂(Me₄en)][f]	C_1	2.070	2.089	2.084	2.063	2.215	2.221	86.94	87.47	82.6	171.99	---	95.5	96.4	88.36
Co(A-B)₂(C-D)	[Co(TTFA)₂(Me₂en)][f]	C_1	2.085	2.061	2.101	2.086	2.224	2.134	88.6	85.7	81.7	172.7	95.6	87.2	90.9	90.4
Co(A-A)₂c₂	[Co(ac)₂(Hdmpz)₂][g]	C_1	2.060	2.098	2.088	2.057	2.166	2.159	88.01	88.63	86.97	171.79	86.93	98.52	98.88	87.62
Co(A-B)₂c₂	[Co(TTFA)₂-(CH₃py)₂] (**4**)	C_2	2.045(4)	2.099(4)	2.099(4)#	2.045(4)#	2.159(5)	2.159(5)#	88.21(15)	88.21(15)#	93.0(3)	178.0(2)	89.11(17)	89.51(17)	89.51(17)#	89.11(17)#

trans(N)-Complexes

		sym.	Co–O1	Co–O2	Co–O3	Co–O4	Co–N1	Co–N2	O1CoO2	O2CoO3	O1CoO3	N1CoN2	N1CoO1	N1CoO2	N2CoO1	N2CoO2
Co(A-A)₂c₂	[Co(HFA)₂(CH₃py)₂] (**3**)[h,i]	C_{2v}	2.060(1)	2.060(1)#	2.060(1)#	2.060(1)#	2.145(3)	2.167(3)	88.54(7)	91.42(7)	177.96(7)	180#	91.02(4)	91.02(4)#	88.98(4)	88.98(4)#
	[Co(ac)₂(Him)₂][h,i]	C_i	2.064	2.064	2.064#	2.064#	2.152	2.152#	88.0	92.0#	180#	180#	87.6	92.1	92.4#	87.9#
	Co(ac)₂(py)₂][j]	C_{2v}	2.034	2.034#	2.034#	2.034#	2.176	2.197	89.8	90.2#	179.2	180#	90.4	90.4#	89.6	89.6#
	[Co(ac)₂(CH₃py)₂][k]	C_{2v}	2.044	2.044#	2.044#	2.044#	2.13	2.18	88.4	91.4	180#	180#	91.2	91.2#	88.7	88.7#
	[Co(ac)₂(Mequin)₂][l]	C_i	2.028	2.043	2.028#	2.043#	2.262	2.262#	89.3	90.7#	180#	180#	89.5	91.9	89.5	91.9
	[Co(tmhd)₂py₂][m]	C_i	2.035	2.037	2.035#	2.037#	2.163	2.163#	87.76	92.24#	180#	180#	91.04	88.92	88.96#	91.08#
Co(A-B)₂c₂	[Co(TTFA)₂(CF₃py)₂] (**5**)	C_i	2.051(2)	2.053(2)	2.051(2)#	2.053(2)#	2.172(3)	2.172(3)#	89.37(9)	90.63(9)#	180#	180#	89.65(9)	88.26(10)	90.35(9)#	91.74(10)
	[Co(bzac)₂(Him)₂][i]	C_i	2.060	2.082	2.060#	2.082#	2.144	2.144#	88.4	91.6#	180#	180#	90.4	89.8	89.6#	90.1#

[a] ac = acetylacetonate; Me₄en = *N,N,N',N'*-tetramethyl-1,2-diaminoethane; Et₄en = *N,N,N',N'*-tetraethyl-1,2-diaminoethane; Me₂en = *N,N*-dimethyl-1,2-diaminoethane; Hdmpz = 3,5-dimethylpyrazole; Him = imidazol; Mequin = 6-Methylquinolin; tmhd = 2,2,6,6-tetramethylhepta-3,5-dionato; bzac = benzylacetonate. [b] For atom numbering, see Figure 3: **1** for *cis*(N) and **3** for *trans*(N) (O2 = O1C, O3 = O1B, O4 = O1A) complexes. [c] Ref 38. [d] Ref 33. [e] Ref 34. [f] Ref 35. [g] Ref 42. [h] Average values, A. U. contain 2 halve molecules. [i] Ref 39. [j] Ref 36. [k] Ref 40. [l] Ref 37. [m] Ref 41. # Resulting from symmetry.
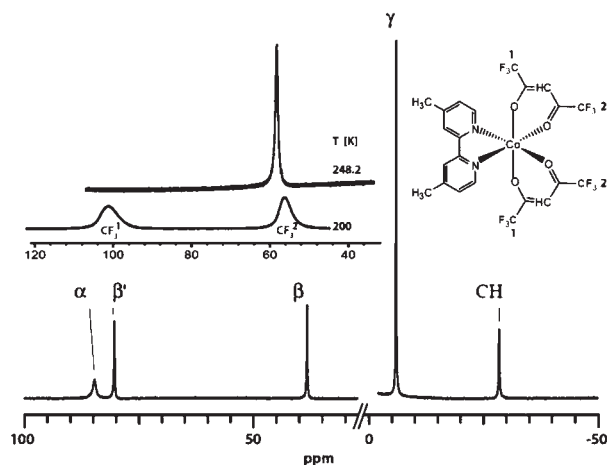
Figure 4. ^{1}H NMR spectrum (400.2 MHz, ref TMS) at 220.1 K of [Co(HFA)$_2$bpic] (**1**) and (insert) ^{19}F NMR spectra (376.3 MHz, ref ext. CF$_3$COOH) at 200 and 248.2 K in CD$_2$Cl$_2$.

corresponds to less distorted octahedral arrangements of the donor atoms in these four *tris*-chelates.

The first two cobalt(II) *bis*-acetylacetonate complexes **1** and **2** have as third chelate a bipyridine type ligand forcing the *cis* arrangement of the two nitrogens donor atoms in octahedral environments. In compounds **3** to **5** the bidentate nitrogen ligand is replaced by two monodentate pyridine type ligands. This opens the possibility of a larger number of isomers involving not only *cis* nitrogens, but also *trans* ones (Figure 2). In this family of Co(II) complexes the *trans* isomers are dominating in solution and are usually obtained in the solid state. The only exceptions are the *cis*(N)-[Co(ac)$_2$(Hdmpz)$_2$]^{35} complex, belonging to the [Co(A-A)$_2$c$_2$] type, and the *cis*(N)-*cis*(CF$_3$)-*trans*(S) isomer [Co(TTFA)$_2$(CH$_3$py)$_2$](V-**4**), belonging to the [Co(A-B)$_2$c$_2$] type (Figure 2 and 3, Table 2). Compared to the strained distorted octahedral structures of **1** and I-**2**, the structures in the two *cis*(N) monodentate ligand complexes are now relaxed and form almost regular octahedral arrangements around the cobalt center. In compound V-**4** the N1−Co−N2 angle is now close to 90° (increase from average 77.8° to 93.0°), and the O−Co−O bite angle of TTFA has increased from 85.9° (average in I-**2**) to 88.2°. The O1−Co−O4 angle (178.0°) is now quasi linear and the O−Co−N angles are close to 90° (average 89.3°). As found in I-**2**, the Co−O(CF$_3$) (distance 2.099 Å) bond strength in V-**4** is also

weaker than the Co−O(thienyl) (2.045 Å) bond strength. The pyridine ring planes are not exactly coplanar (deviation of 34.1°) with the corresponding CoO$_3$ planes.

The *trans*(N) complexes in Table 2 belong to the C_{2v} or to the C_i point group of symmetry. For symmetry reason the N−Co−N angle is always 180°, and the N−Co−O angles deviate only slightly from 90° (less than 2°), ensuring an almost perfect octahedral symmetry for all this family of complexes. The most frequently found structures belong to the *trans*(N)-[Co(A-A)$_2$c$_2$] type: [Co(HFA)$_2$-(CH$_3$py)$_2$](*trans*-**3**) (C_{2v}), [Co(ac)$_2$(Him)$_2$]^{39} (C_i), [Co(ac)$_2$-(py)$_2$]^{36} (C_{2v}), [Co(ac)$_2$(CH$_3$py)$_2$]^{40} (C_{2v}), [Co(ac)$_2$-(Mequin)$_2$]^{37} (C_i), [Co(tmhd)$_2$py$_2$]^{41} (C_i). In the three C_{2v} complexes the Co−N1 and Co−N2 distances differ only slightly indicating, together with the N1−Co−O (average 90.9°) and N2−Co−O (average 89.1°), angle values close to 90°, a very slight out of oxygen plane central Co atom (0.01 Å for **3**). Similarly to [Co(ac)$_2$(CH$_3$py)$_2$],^{40} the two six-member metallocycles of *trans*-**3** have a "boat" conformation with a fold angle along the O−O lines toward the N2 atom equal to 15.3° (Supporting Information, Figure S3). This distortion is probably caused by the CH--π interaction between the proton in the α-position of the pyridine rings and the delocalized π orbital of the six-member metallocycles. The aromatic rings of CH$_3$py are practically perpendicular to the plane of the oxygen donor atoms and orthogonal between themselves, with the N1 pyridine ring bisecting each metallocycle ring and the N2 pyridine ring bisecting the two metallocycle rings. Molecular packing is sustained by multiple CH(py)--F and CH(py)--π(py) interactions.

Both [Co(TTFA)$_2$(CF$_3$py)$_2$](III-**5**) and [Co(bzac)$_2$-(Him)$_2$]^{39} belong to the [Co(A-B)$_2$c$_2$] type complexes with two asymmetric β-diketonate ligands. Among the five possible isomers both complexes have a *trans*(N)-*trans*-(CF$_3$ or bz) configuration (Figure 2). The high symmetric octahedral coordination polyhedron around Co in compound III-**5** (C_i) is quite similar to III-**3** (C_{2v}). The main differences being the *"chair"* conformation of the two six-member metallocycles (angle of the planes along the O−O line: 18.5°) and the parallelism of the aromatic rings of CF$_3$py, which are now both bisecting the O1−Co−O2A and O1A−Co−O2 angles in III-**5**.

3.2. Solution Structure and Isomerization Kinetics of Mixed Ligand *tris*-Chelates Complexes. To gain a maximum information on the isomerization mechanism of cobalt(II) *tris*-chelates, we have chosen to study complexes with mixed bidentate ligands including asymmetric ligands (Figure 2). The symmetric HFA and the asymmetric TTFA acetylacetonate ligands are negatively charged, and the symmetric bpic and bpy pyridine ligands are neutral. This composition has the advantage to lead to neutral complexes well soluble in dichloromethane, allowing to work at the low temperatures required to study the highly stereolabile cobalt(II) complexes. All of them are strongly paramagnetic with the $S = 3/2$ high spin configuration and have a large spin orbital contribution because of the low crystal field created by the four oxygen and the two nitrogen atoms. This property has the convenience to produce very large chemical shifts, with comparatively small paramagnetic line-broadenings,^{43}

(33) Colborn, R. E.; Garbauskas, M. F.; Hejna, C. I. *Inorg. Chem.* **1988**, *27*, 3661–3663.

(34) Tzavellas, L. C.; Tsiamis, C.; Kavounis, C. A.; Cardin, C. J. *Inorg. Chim. Acta* **1997**, *262*, 53–59.

(35) Tanase, S.; Bouwman, E.; Reedijk, J.; Driessen, W. L.; Ferbinteanu, M.; Huber, M.; Mills, A. M.; Spek, A. L. *Eur. J. Inorg. Chem.* **2004**, 1963–1969.

(36) Elder, R. C. *Inorg. Chem.* **1968**, *7*, 1117–1123.

(37) Hursthouse, M. B.; Malik, K. M. A.; Davies, J. E.; Harding, J. H. *Acta Crystallogr., Sect. B* **1978**, *34*, 1355–1357.

(38) Pasko, S.; Hubert-Pfalzgraf, L. G.; Abrutis, A.; Vaissermann, J. *Polyhedron* **2004**, *23*, 735–741.

(39) Döring, M.; Ludwig, W.; Uhlig, E.; Wocadlo, S.; Müller, U. *Z. Anorg. Allg. Chem.* **1992**, *611*, 61–67.

(40) Gulya, A. P.; Novitskii, G. V.; Shova, S. G.; Mazus, M. D.; Sandu, I. *Koord. Khim.* **1993**, *19*, 227–231.

(41) Santhosh, K.; Gnanou, Y.; Champouret, Y.; Daran, J.-C.; Poli, R. *Chem.—Eur. J.* **2009**, *15*, 4874–4885.

(42) Marsh, R. E. *Acta Crystallogr., Sect. B* **1997**, *53*, 317–322.

(43) Bertini, I.; Luchinat, C.; Parigi, G. *Solution NMR of Paramagnetic Molecules*; Elsevier: Amsterdam, The Netherlands, 2001; Vol. *2*.

Table 3. Equilibrium Constants, Thermodynamic Parameters, Rate Constants, and Activation Parameters for the Isomerization Reactions of [Co(HFA)$_2$bpic] (**1**) and [Co(TTFA)$_2$bpy] (**2**) in CD$_2$Cl$_2$

	thermodynamic			kinetic			
	[Co(TTFA)$_2$bpy] (**2**)			[Co(HFA)$_2$bpic] (**1**)	[Co(TTFA)$_2$bpy] (**2**)		
	II→I	V→II		Δ-**1**→Λ-**1**[a]	Δ-II→Λ-II[a]	I→V	II→V
K^{190}	2.52	1.24	$k^{190}/10^3$ s^{-1}	1.97 ± 0.2	6.6 ± 0.7	1.4 ± 0.2	0.03 ± 0.02
K^{265}	1.74	0.82	$k^{265}/10^3$ s^{-1}	1510 ± 150	871 ± 219	403 ± 101	14 ± 6
$\Delta H°$/kJ mol^{-1}	−2.07 ± 0.06	−2.28 ± 0.06	$\Delta H^{\ddagger}$/kJ mol^{-1}	35.23 ± 0.7	25.4 ± 1.3	29.7 ± 1.3	32.7 ± 4
$\Delta S°$/J K^{-1} mol^{-1}	−3.2 ± 0.3	−10.2 ± 0.3	$\Delta S^{\ddagger}$/J K^{-1} mol^{-1}	+7.3 ± 2.5	−34.3 ± 6	−24.6 ± 6	−41.2 ± 17
			$\Delta V^{\ddagger}$/cm^3 mol^{-1}	+7.5 ± 1 [b]			

[a] Enantiomerization. [b] At 253 K, $k/10^3$ s^{-1} = 595 ± 80.

which allows the detection of short lifetime ($\tau < 10^{-6}$ s) cobalt(II) isomeric species.[16]

[**Co(HFA)$_2$bpic**] (**1**). The complex **1** belongs to the [Co(A-A)$_2$(C-C)] family of *tris*-chelates, with 2 isomers forming a chiral pair (Figure 2). The two enantiomers Δ-**1** and Λ-**1** cannot be distinguished by NMR unless the ligands are chiral. The ^{1}H NMR spectrum (Figure 4) shows five resonances for **1** at 220.1 K corresponding to the α, β′, β, and γ protons of bpic and the CH proton of HFA (integrals in parentheses): 86.1(1), 79.3(1), 42.4(1), 6.2(3), and −28.2(1) ppm. The two CF$_3$ groups, labeled 1 (*trans* to O) and 2 (*trans* to N), are magnetically non-equivalent as shown in the ^{19}F NMR spectrum at 194.7 K. Raising the temperature leads to the coalescence of these two signals. As expected no dynamic phenomenon is observed in the ^{1}H NMR spectrum between 180 and 300 K.

The temperature dependent ^{19}F NMR spectra were analyzed as an exchange between the two equally popu-lated CF$_3$(1) and CF$_3$(2) sites using the line-width of both signals at low temperature and fitting the experimental spectra with the Kubo−Sack calculated spectra at higher temperature (Supporting Information, Table S2). The variation of the chemical shifts with temperature was taken into account, as well as the small paramagnetic contributions to the transverse relaxation (Figures 5(i) and 5(ii)). The variable temperature study has been extended by variable pressure ^{19}F NMR experiments at 253.2 K, up to 200 MPa, on the already coalesced signals (Figure 5(iii) and Supporting Information, Figure S4). At this temperature the paramagnetic contribution to the transverse relaxation rate $1/T_2$ is small ($\approx 12\%$): a varia-tion between −4 and +4 cm^3 mol^{-1} of $\Delta V^{\ddagger}_{para}$ does not modify $\Delta V^{\ddagger}_{kin}$ for the interconversion process by more than its experimental accuracy. The rates and activation parameters for this process are reported in Table 3. The mechanistic assignment for the CF$_3$(1)$\leftrightarrow$CF$_3$(2) intercon-version (Bailar twist, Rây−Dutt twist, bidentate ligand TBP or SQ dissociation) cannot be made at this stage, but will be discussed below together with the *tris*-chelate **2**.

[**Co(TTFA)$_2$bpy**] (**2**). This complex belongs to the [Co(A-B)$_2$(C-C)] family of *tris*-chelates forming six iso-mers consisting in three chiral pairs (Figure 2). For simplification the pair of isomers (the CF$_3$ are magneti-cally equivalent in the Δ and Λ pairs) are designated by **I** for *trans*(CF$_3$), **II** for *cis*(CF$_3$)-*cis*(S), and by **V** for *cis*(CF$_3$)-*trans*(S). The variable temperature ^{19}F NMR spectra (Figure 6) are indicative of a fast dynamic equilibrium between the three chiral pairs. At 200 K, the exchange rates are slow enough to allow the observation
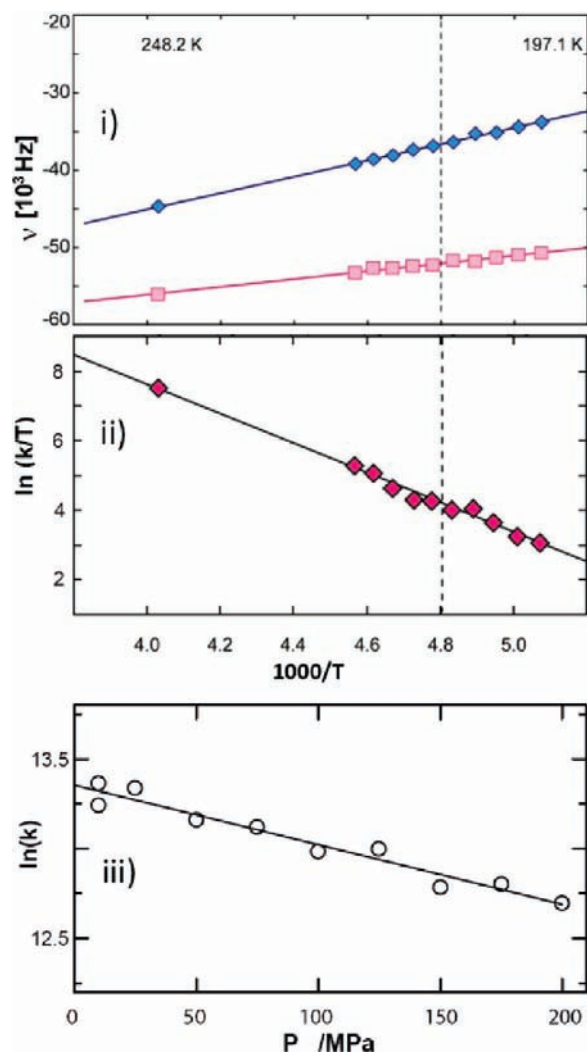
Figure 5. Kinetics of the Δ-**1**↔Λ-**1** enantiomerization of [Co(HFA)$_2$-bpic] (**1**) followed by ^{19}F NMR in CD$_2$Cl$_2$: resonance frequencies (i) and rate constants as a function of temperature (ii), and as function of pressure at 253.2 K (iii). Vertical broken lines are used to separate data obtained using Lorentzian fitting of the signals at low *T* and Kubo−Sack spectral analysis at high *T*.

of the single signals of **I** and **V**, and the two signals **II**-1 (*trans* to O) and **II**-2 (*trans* to N) of the isomer **II**. The assignments are based on the equal population of **II**-1 and **II**-2, the distribution of the isomers with dielectric constant (polar isomers are favored in higher ε solvent), and by comparison with *bis*-chelates to be discussed later. At higher temperature the four signals finally coalesce to a single signal.
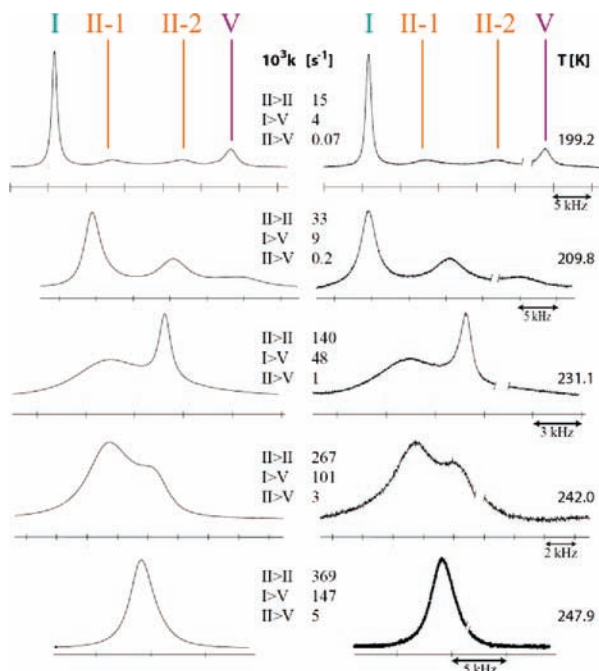
Figure 6. Selection of experimental (right) and Kubo–Sack calculated (left) ^{19}F NMR spectra of $[Co(TTFA)_2bpy]$ (**2**) in CD_2Cl_2 (ref $CFCl_3$, deleted in the figure).

The isomerization process has been analyzed using the ^{19}F NMR spectra. Starting at low temperature the well separated CF_3 signals have been analyzed as Lorentzians, giving access to the variation with temperature of the paramagnetic transverse relaxation rates, the chemical shifts, and the population of the four sites. Upon increasing the temperature the isomerization kinetics become too fast and necessitates a Kubo–Sack full line-shape analysis with an exchange matrix written for four possible twist interconversions: $\mathbf{I} \leftrightarrow \mathbf{II}$, $\mathbf{II} \leftrightarrow \mathbf{V}$, $\mathbf{I} \leftrightarrow \mathbf{V}$, and $\mathbf{II}\text{-}1 \leftrightarrow \mathbf{II}\text{-}2$ (Table 3 and Supporting Information, Table S3).[2] Visually it is clear that two exchange processes are dominating: $\mathbf{II}\text{-}1 \leftrightarrow \mathbf{II}\text{-}2$ and $\mathbf{I} \leftrightarrow \mathbf{V}$ (Figure 6). If these were the only processes the high temperature spectra would show two signals, but a single signal is observed above 245 K. This requires a small contribution of the $\mathbf{II} \leftrightarrow \mathbf{V}$ and/or $\mathbf{I} \leftrightarrow \mathbf{II}$ isomerization paths at high temperature. It is not possible from the simulation to decide between these two contributions. Arbitrarily we decided to simulate the spectra by adding the $\mathbf{II} \leftrightarrow \mathbf{V}$ path. The temperature evolution of the chemical shifts and of the population of the species, and of the isomerization rate constants are given in Figure 7. The corresponding equilibrium constants, thermodynamic parameters, and activation parameters for the isomerization processes are reported in Table 3.
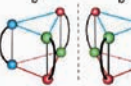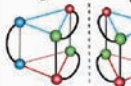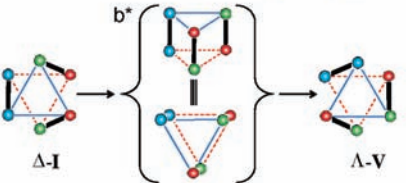
At 158.9 K in CD_2Cl_2 the isomer **I** of $[Co(TTFA)_2bpy]$ (**2**) is by far the most populated: 67.4% for **I**, 20.2% for **II**, and 12.3% for **V** (Figure 7). In conformity with this observation it is the $trans(CF_3)$-$[Co(TTFA)_2bpy]$ isomer which is obtained from crystallization in CH_2Cl_2. Raising the temperature to 279.8 K leads to a decrease of the population of the $trans(CF_3)$ isomer **I** (41.8%) and an increase of the population of both $cis(CF_3)$ isomers (25.6% for **II** and 32.6% for **V**). The equilibrium constants and thermodynamic parameters for the isomerization reactions are reported in Table 3.
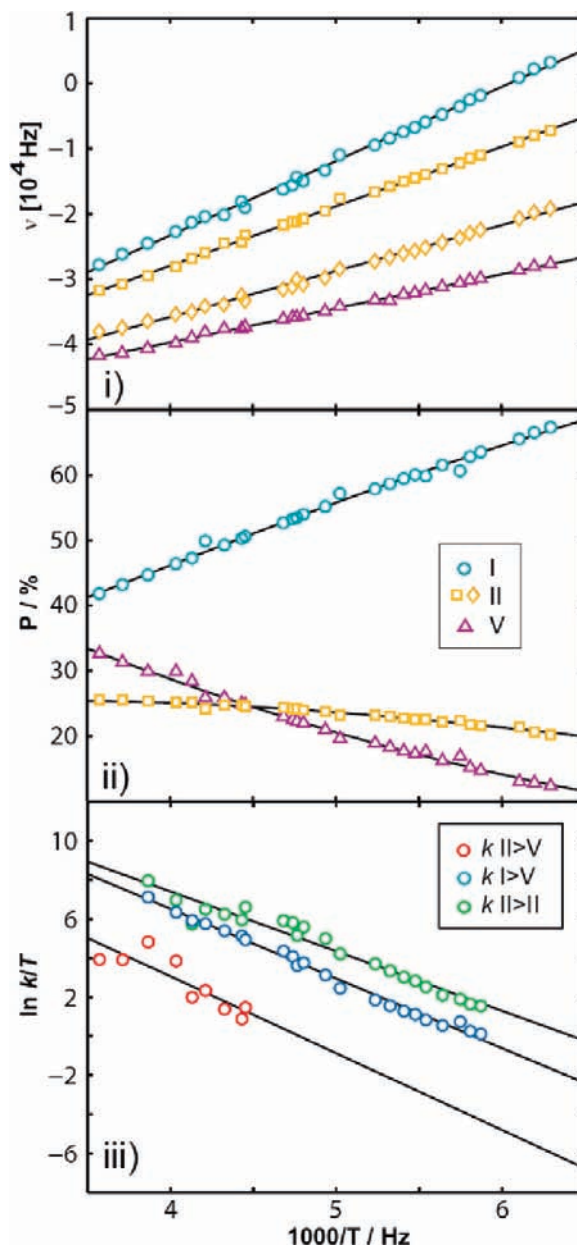
Figure 7. Kinetics of isomerization between the 3 pairs of enantiomers of $[Co(TTFA)_2bpy]$ (**2**) followed by ^{19}F NMR in CD_2Cl_2: resonance frequencies (i), populations (ii), and rate constants (iii). In the slow exchange domain (160–188 K) the spectra were analyzed by Lorentzian fitting, and in the intermediate and fast exchange domains (191–280 K) a Kubo–Sack spectral analysis was performed. A stack plot of selected spectra is shown in the Supporting Information, Figure S4.

The mechanisms with A-B or C-C dissociative ring-opening of $[Co(A\text{-}B)_2(C\text{-}C)]$ through TBP-axial and TBP-equatorial intermediates do not allow the direct $\mathbf{I} \leftrightarrow \mathbf{V}$ interconversion (see Figure 38 of ref 2), which eliminates these as a possible isomerization mechanisms. The A-B ligand ring-opening through SP intermediates does allow all possible interconversions $\mathbf{I} \leftrightarrow \mathbf{II}$, $\mathbf{II} \leftrightarrow \mathbf{V}$, $\mathbf{I} \leftrightarrow \mathbf{V}$, and $\mathbf{II}\text{-}1 \leftrightarrow \mathbf{II}\text{-}2$, whereas the C-C ligand ring-opening through SP intermediates only allows $\mathbf{I} \leftrightarrow \mathbf{V}$ and $\mathbf{II}\text{-}1 \leftrightarrow \mathbf{II}\text{-}2$ interconversions (see Figure 39 of ref 2). Therefore the SP dissociative mechanisms cannot be eliminated at this stage as simply as the TBP dissociative mechanisms, but they are considered as energetically less favorable than the twist

Table 4. Twist Isomerization Pathways and Intermediates for [Co(A-A)$_2$(C−C)] and [Co(A-B)$_2$(C−C)] Complexes.[a]

Isomerization reaction	Transition states		Rate Constants $k^{265}/10^3$ s^{-1}
	Bailar trigonal path	*Râ_y-Dutt* rhombic path	
[Co(A-A)$_2$(C-C)]	Δ−1 $\underset{a,b,c}{\rightleftharpoons}$ Λ−1		[Co(HFA)$_2$bpic] (**1**)
Δ-1 ↔ Λ-1	*a*	*c* *b*	1510 ± 150
[Co(A-B)$_2$(C-C)]	I $\xrightarrow{f}$ $\begin{bmatrix} Δ−II \\ \updownarrow a,c \\ Λ−II \end{bmatrix}$ $\updownarrow b,d$ V $\xrightarrow{e}$		[Co(TTFA)$_2$bpy] (**2**)
Δ-II ↔ Λ-II	*a*	*c*	871 ± 219
Δ-I ↔ Λ-V, Λ-I ↔ Δ-V	*b* *b**	*d* *d**	403 ± 101
Δ-II ↔ Λ-V, Λ-II ↔ Δ-V	-	*e* *e**	14 ± 6
Δ-I ↔ Λ-II, Λ-I ↔ Δ-II	-	*f* *f**	zero
Example:		*b** Δ-I → {...} → Λ-V	

[a] The respective NMR exchange matrices are given in Supporting Information, Tables S2 and S3.

mechanisms which do not require bond-breaking. The twist isomerization paths for the mixed *tris*-chelate complexes are reported in Table 4. There are 3 possible prismatic intermediates for the Δ ↔ Λ enantiomerization of the complexes [Co(A-A)$_2$(C-C)] and 10 possible prismatic intermediates for the 4 interconversion processes of the complexes [Co(A-B)$_2$(C-C)]. For the latter family there are 4 chiral pairs and two achiral prismatic intermediates. The isomerization paths are classified in two categories according to the geometry of the intermediates: the Bailar twist with trigonal intermediates and the Râ_y−Dutt twist with rhombic intermediates (Figure 1). The two isomerization paths Δ-II ↔ Λ-II and I ↔ V can occur according to both mechanisms, whereas the two other paths, I ↔ II and II ↔ V, can only take place by the Râ_y−Dutt twist mechanism. For the complex [Co(TTFA)$_2$bpy] (**2**) the Δ-II ↔ Λ-II and I ↔ V and paths are strongly kinetically favored, compared to the I ↔ II and II ↔ V paths (Table 3). On the basis of this comparison we favor a Bailar twist mechanism for the isomerization reactions. For the single pair of enantiomers of [Co(HFA)$_2$bpic] (**1**) both twist mechanisms are feasible, but we again suggest that the mechanism is a Bailar twist by analogy with that observed for complex **2**, further supported by the similarity of their interconversion rate constants. The small positive values of the entropy and the volume of activation for the enantio-merization path of **1** ($\Delta S^{\ddagger}$: +7.3 J K^{-1} mol^{-1}; $\Delta V^{\ddagger}$: +6.9 cm^3 mol^{-1}) and the negative values of the entropy of activation for

the three isomerization paths of **2** ($\Delta S^{\ddagger}$: −34.3, −24.6, −41.2 J K^{-1} mol^{-1}) are consistent with the assignment of a twist versus a ring-opening mechanism for the isomerization of these two Co(II) mixed ligand *tris*-chelates. Notice that whatever the twist mechanism, each isomerization is accompanied by an enantiomerization.

The arbitrary choice of the **II ↔ V** pathway, and not **I ↔ II**, in the fitting procedure was made because it has the highest chemical shift difference (Figure 7i). The same fittings and calculation performed using the **I ↔ II** path-way would lead to a similar $\Delta H^{\ddagger}$ value, but an equal or more negative $\Delta S^{\ddagger}$ value. We cannot conclude to the operation of the first, the second, or simultaneously both pathways. However, the clearly negative $\Delta S^{\ddagger}$ value allows to exclude a dissociative activated process. The Bailar twist is not possible for both pathways (Table 4); we can therefore conclude to a Râ_y−Dutt rhombic twist operat-ing for this(ese) process(es).

3.3. Solution Structure and Isomerization Kinetics of *bis*-Bidentate Chelate Complexes. Neutral complexes of the type [Co(A-A)$_2$c$_2$] and [Co(A-B)$_2$c$_2$] may exist as *trans* and *cis* isomers, the *cis* isomers being optically active. Compared to the *tris*-chelates there is added complexity reflected by the increased number of isomers, the numerous isomerization pathways, and the observa-tion of coordinated/free monodentate ligand exchange reactions.
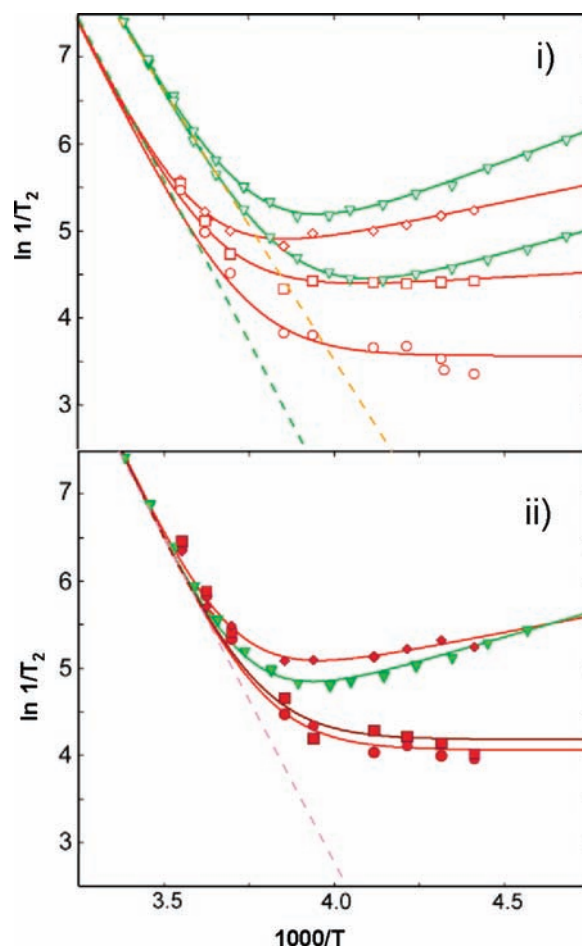
Table 5. Equilibrium Constants, Thermodynamic Parameters, Rate Constants, and Activation Parameters for the Isomerization Reactions of [Co(HFA)$_2$(CH$_3$py)$_2$] (**3**) in CD$_2$Cl$_2$ (214−295 K; [complex]/[free CH$_3$py] = 1:7)

	thermodynamic		kinetic				
	cis→*trans*		Δ-*cis*→Λ-*cis*[a]	*cis*→*trans*	*trans*→*cis*	*trans*→L[b]	*cis*→L[b]
$K_{c,t}^{265}$	0.42 ± 0.01	k^{265}/s^{-1}	84	26	61	≤1.5	≤5.9
$K_{c,t}^{298}$	0.34 ± 0.01	k^{298}/s^{-1}	1284	728	2093	≤49	≤278
$\Delta H°_{c,t}$/kJ mol^{-1}	−4.05 ± 0.15	$\Delta H^{\ddagger}$/kJ mol^{-1}	51.76 ± 3	63.96 ± 3	67.75 ± 3		
$\Delta S°_{c,t}$/J K^{-1} mol^{-1}	−22.5 ± 0.6	$\Delta S^{\ddagger}$/J K^{-1} mol^{-1}	−11.8 ± 15	+24.4 ± 15	+45.9 ± 15		
$\Delta V°_{c,t}$/cm^3 mol^{-1}	−1.5 ± 1	$\Delta V^{\ddagger}$/cm^3 mol^{-1}	+2.4 ± 1	+5.1 ± 1	+6.2 ± 1		

[a] Enantiomerization. [b] *trans* and *cis* coordinated CH$_3$py/free CH$_3$py exchange.
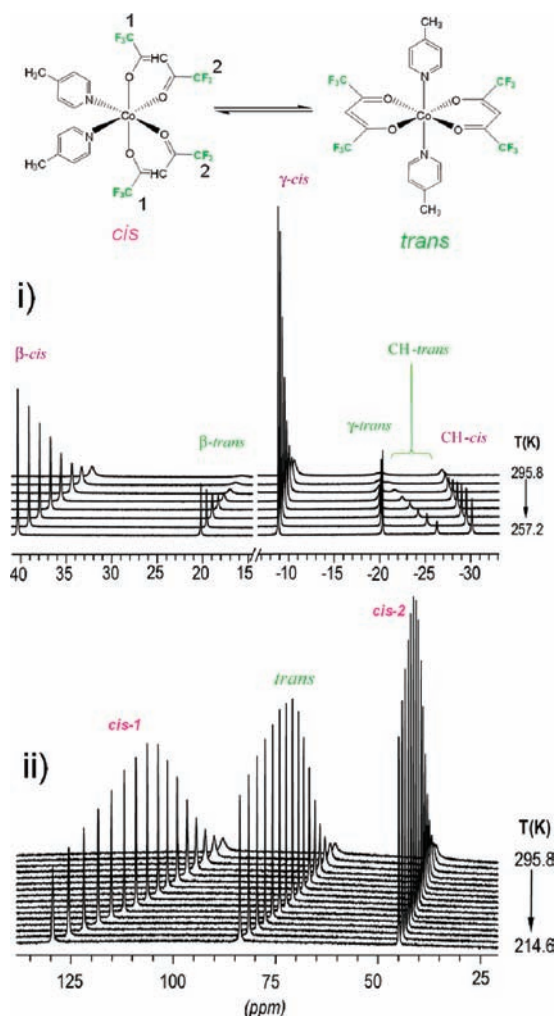
Figure 8. ^{1}H NMR (i) and ^{19}F NMR (ii) spectra of [Co(HFA)$_2$-(CH$_3$py)$_2$] (**3**) as a function of temperature in CD$_2$Cl$_2$ ([complex]/[free CH$_3$py] = 1:7 ; refs TMS and ext. CF$_3$COOH).

Figure 9. Experimental and fitted transverse relaxation rates $1/T_2$ of the (i) *cis* and (ii) *trans* isomers of [Co(HFA)$_2$(CH$_3$py)$_2$] (**3**) from 214.0 to 295.8 K in CD$_2$Cl$_2$ ([complex]/[free CH$_3$py] = 1:7). ^{1}H and ^{19}F NMR values are in red and green, respectively: for the β (open and solid red squares) and γ (open and solid red circles) signals of CH$_3$py, and the CH (open and solid red diamonds) and CF$_3$ (open and solid green triangles) signals of HFA. The dashed lines indicate the kinetic contributions ($k_{c\rightarrow t}$: red dashed lines, $k_{\Delta\text{-}c\rightarrow\Lambda\text{-}c} + k_{t\rightarrow c}$: green dashed lines, $k_{t\rightarrow c}$: red dashed lines).

[Co(HFA)$_2$(CH$_3$py)$_2$] (3). The simplest complex of the family of *bis*-bidentate chelates is the [Co(A-A)$_2$c$_2$] type (Figure 2). It can exist with the two monodentate ligands in *trans* and in *cis* positions. The latter is in the form of two diastereoisomers, not distinguishable by NMR unless the ligands are themselves chiral. Representative ^{19}F NMR spectra of **3** are reported as a function of temperature in Figure 8. The two equally populated CF$_3$ signals at +44.8 ppm and +129.6 ppm are assigned to the *cis* isomer and the CF$_3$ signal at +84.2 ppm to the *trans* isomer (214.6 K). The ^{1}H NMR spectra of the same solution show six signals apart from the signals of the free ligand

(not shown). Their assignments are based on the integrals, the comparison with the ^{19}F NMR spectra, and the proximity to the paramagnetic center. The signals at +40.9 (β-*cis*), −9.4 (γ-*cis*), and −30.2 (CH-*cis*) ppm belong to the *cis* isomer and those at +20.3 (β-*trans*), −20.2 (γ-*trans*), and +26.5 (CH-*trans*) ppm to the *trans* isomer (257.2 K). The ^{1}H and ^{19}F NMR integrals were used to obtain the isomerization equilibrium constant $K_{c,t}$ = [*trans*]/[*cis*] as function of temperature in CD$_2$Cl$_2$ and to calculate the corresponding thermodynamic parameters $\Delta H°_{c,t}$ and
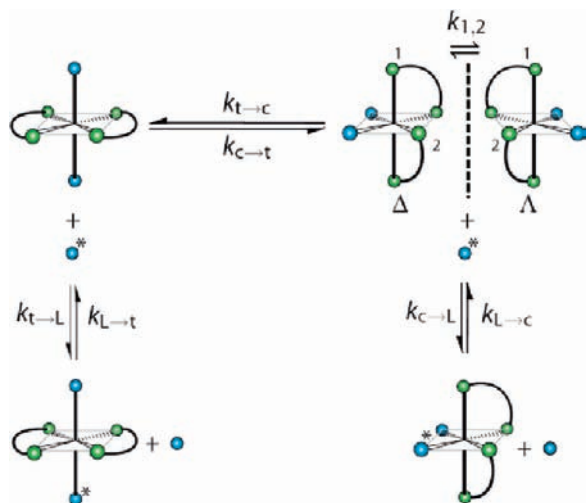
**Figure 10.** *trans*-**3**/*cis*-**3** isomerization, Δ-*cis*-**3**/Λ-*trans*-**3** enantiomerization, and coordinated/free CH$_3$py reaction pathways of [Co(HFA)$_2$-(CH$_3$py)$_2$] (**3**) in the presence of an excess of CH$_3$py in CD$_2$Cl$_2$.

ΔS°$_{c,t}$ (Table 5 and Supporting Information, Figure S6). The *cis* isomer is favored at low temperature, and both isomers become equally populated around 270 K. Notice that the *trans* isomer is obtained by recrystallization from MeOH.

For the *bis*-bidentate chelate [Co(HFA)$_2$(CH$_3$py)$_2$] (**3**) the isomerization rates are much slower than for the *tris*-chelates **1** and **2** described previously. The ^{1}H and ^{19}F signals are well separated over the temperature range (214.0 to 295.8 K) accessible in CD$_2$Cl$_2$. The inverse of the transverse relaxation rates $1/T_2$ were directly obtained by simple Lorentzian line-shape analysis (Figure 9). The $1/T_2$ behaviors are characteristic of a paramagnetic contribution dominating at low temperature and a kinetic contribution dominating at higher temperatures, and they were described by Arrhenius and Eyring equations, respectively. The study performed in the presence of an excess of free CH$_3$py gives access to the rates of *cis*/*trans* and Δ-*cis*/Λ-*cis* isomerizations, and to the intermolecular coordinated/free CH$_3$py exchange (Figure 10 and Supporting Information, Table S4). In the kinetic temperature domain the line broadening is only due to both isomerization processes in ^{19}F NMR, whereas in ^{1}H NMR the *cis*/*trans* isomerization and the coordinated/free ligand exchange are contributing. The simultaneous analysis of the ^{1}H and ^{19}F transverse relaxation rates leads to the kinetic parameters reported in Table 5. The fastest process is the Δ-*cis*/Λ-*cis* enantiomerization, followed by the *cis*/*trans* isomerization. Finally, the intermolecular coordinated/free ligand exchanges represent at most 10% of the kinetic broadening, and therefore only maximum limits for these rate constants can be reported.

The effects of pressure on the thermodynamic and the kinetic parameters for the *cis*/*trans* isomerization and the Δ−*cis*/Λ−*cis* enantiomerization of **3** were obtained by simultaneous fitting of the populations of the *cis* and *trans* isomers and of the ^{19}F transverse relaxation rates as a function of pressure (up to 200 MPa) at 296.3 K (Supporting Information, Figure S7). At this temperature the paramagnetic contribution to the transverse relaxation rates is less than 5%. The corresponding reaction
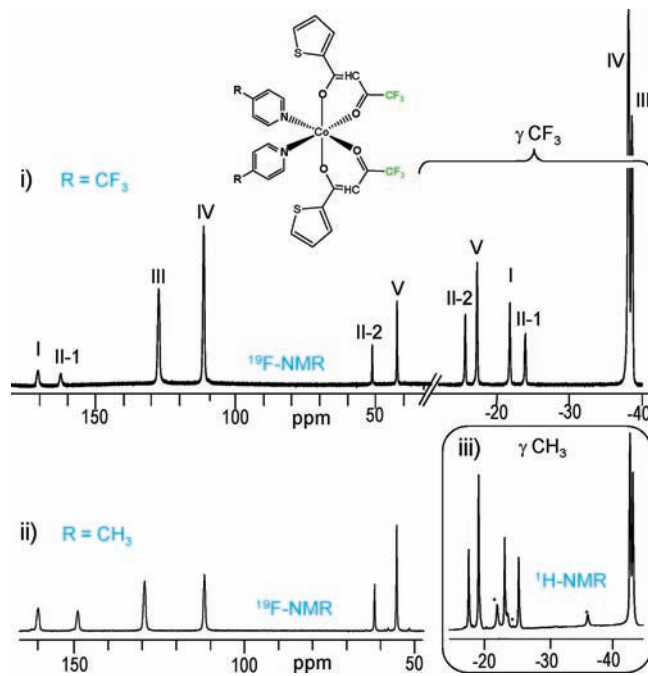
Figure 11. Comparison of the ^{19}F NMR spectrum of 25 mM [Co(TTFA)$_2$(CF$_3$py)$_2$] (**5**) (i) and the ^{19}F NMR (ii) and the ^{1}H NMR (iii) spectra of 25 mM [Co(TTFA)$_2$(CH$_3$py)$_2$] (**4**) at ~230 K in CD$_2$Cl$_2$ (ext. ref CF$_3$COOH). The signal of excess free amine is suppressed. The formula drawn is the isomer Δ-**V**: Δ-*cis*(N)-*cis*(CF$_3$)-*trans*(S). * Signals of the CH group of TTFA.

volumes ΔV°$_{c,t}$ and activation volumes ΔV‡$_{\Delta c > \Lambda c}$ and ΔV‡$_{c > t}$ are reported in Table 5.

[Co(TTFA)$_2$(CH$_3$py)$_2$] (4) and [Co(TTFA)$_2$(CF$_3$py)$_2$] (5). These complexes of the [Co(A-B)$_2$c$_2$] type are of stereochemical interest since they can possibly exist in eight isomeric forms, three chiral pairs of isomers which have the monodentate c-ligands in *cis*-position to each other and two achiral isomers with the c-ligands in *trans*-position (Figure 2). The low temperature (230 K) NMR spectra of complexes **4** and **5** in CD$_2$Cl$_2$ with added free CH$_3$py are shown in Figure 11. The resemblance of the spectra of both complexes simplified the assignment of their NMR signals which is based on a detailed previous investigation of **4**.[20] The six high frequency ^{19}F signals belong to the CF$_3$ group of TTFA. The three *cis*(N) isomers (**I**, **II**, and **V**) exist in two enantiomeric forms (Δ and Λ) not distinguishable by NMR (Figure 2). The isomer **II** has two equal intensity signals, **II**-1 and **II**-2, corresponding to the magnetically non-equivalent CF$_3$ group of TTFA. The two achiral *trans* isomers show each a single signal. The γ-CH$_3$ and γ-CF$_3$ groups of the five isomers of **4** and **5** lead also to six ^{1}H, respectively, ^{19}F NMR signals. The isomers **II** have again two equal intensity signals corresponding to the groups *trans* to the thienyl or CF$_3$ fragment of TTFA.

Raising the temperature of the solution of complex [Co(TTFA)$_2$(CH$_3$py)$_2$] (**4**) from 185 to 312 K leads first to a line narrowing of the ^{1}H and ^{19}F NMR signals, with a minimum around 235 K (similarly to the behavior of [Co(HFA)$_2$(CH$_3$py)$_2$] (**3**) in Figure 9), followed by a kinetic line broadening. In this low temperature range, simple Lorentzian line-shape analyses were used to obtain resonance frequencies, populations, and transverse relaxation

rate values. These data allowed to calculate preliminary values for the thermodynamic and kinetic isomerization parameters. Further increase of temperature leads to coalescence and finally a single signal at 312 K. In the high temperature range the Kubo–Sack formalism was used to fit the NMR spectra. To construct the exchange matrix one has to consider the possible isomerization routes: the twist, the dissociation of the monodentate ligand, the bond rupture of one arm of the bidentate ligand (the arm supporting the CF_3 group). These routes are shown in Figure 12, and the corresponding exchange matrices are reported in Supporting Information, Table S5 (see also Chapter IV-B of ref 2).

The exchange matrix describing the twist mechanism did not allow simulating the experimental spectra: the two fast coalescences of the two signals of isomer **II** and of the signal of isomer **I** with that of isomer **V** were not observed. The isomerizations of **4** involve therefore likely
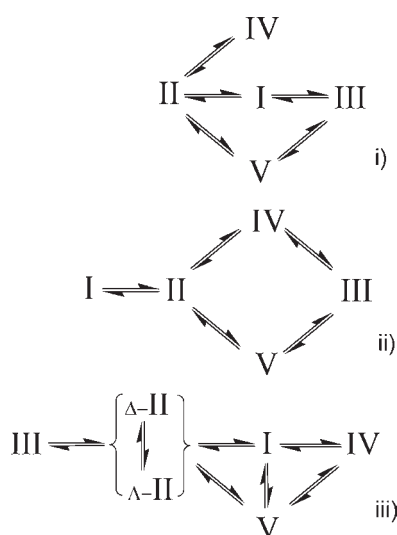

Figure 12. Possible isomerization pathways of the 5 isomers of a *bis*-chelate [Co(A-B)$_2$c$_2$]: mechanism with dissociation of the monodentate ligand c (i), with dissociative ring-opening of an arm of the bidentate ligand A-B (ii), and of the twist type (iii).

a dissociative mechanism. For both dissociative mechanisms (monodentate and bidentate ligand dissociation) four pathways are identical: **I ↔ II**, **II ↔ IV**, **II ↔ V**, and **III ↔ V**. However, the pathway **I ↔ III** is only present in the mechanism involving the dissociation of the monodentate ligand. On the reverse, the pathway **III ↔ IV** can only be found in the mechanism involving the ring-opening of the bidentate ligand. Practically it was found that the **I ↔ III** pathway could be ignored in the spectral analysis without alteration of the quality of the fits, whereas, it was not possible to simulate the spectra in the whole temperature domain and to ignore the most frequent pathway **III ↔ IV**. Some experimental and calculated spectra using the bidentate A-B ligand TBP ring-opening mechanism matrix are shown in Figure 13. Both the real (absorption spectra) and the imaginary (dispersion spectra) parts of the spectra were used in the fitting procedure to minimize the phasing problem (Supporting Information, Figure S1). For simplification only the real parts are given in Figure 13. The ^{19}F NMR frequencies, the mole fractions of the isomers used in the calculations, and the resulting rate constants are shown in Figure 14. The thermodynamic and kinetic parameters of the bidentate A-B ligand TBP ring-opening isomerization processes of [Co(TTFA)$_2$(CH$_3$py)$_2$] (**4**) are summarized in Table 6. The possible participation of the monodentate ligand dissociation in the isomerization mechanism was also checked by comparison of the kinetic line broadening of the CF$_3$ ^{19}F signals of TTFA (only sensitive to the isomerization) with the CH$_3$ ^{1}H signals of CH$_3$py (sensitive to both isomerization and coordinated/free monodentate ligand exchange). Practically this means adding a kinetic term to each entry of the exchange matrix to describe the intermolecular CH$_3$py exchange. No supplementary term is necessary for the three *cis* isomers, indicating the absence of intermolecular ligand exchange on these species. The addition of a small kinetic term slightly improves the simulation the ^{1}H NMR signals of the two *trans* isomers (Supporting Information, Figure S8). This small contribution, too small to determine activation parameters, can be neglected and
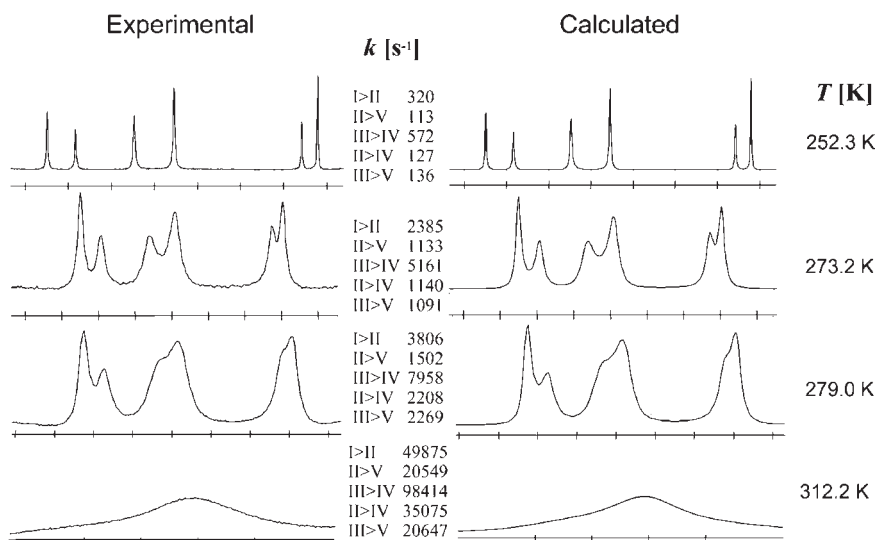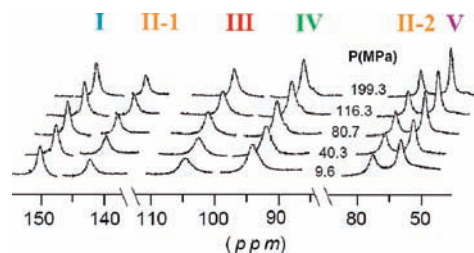

Figure 13. Selection of experimental (left) and Kubo–Sack calculated (right) ^{19}F NMR spectra of [Co(TTFA)$_2$(CH$_3$py)$_2$] (**4**) in CD$_2$Cl$_2$ ([complex]/[free CH$_3$py] = 1:3.5).
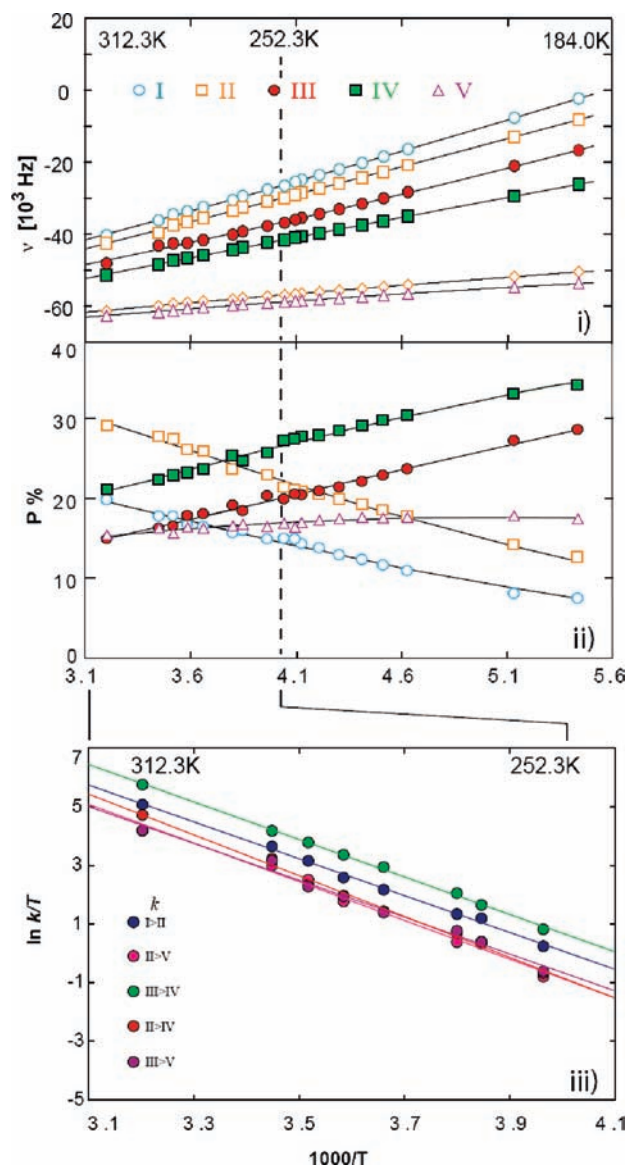
Figure 14. Resonance frequencies ν (i) and mol fractions P (ii) obtained by Lorentzian fitting (right: slow exchange) or by Kubo–Sack fitting (left: intermediate and fast exchange) of the ^{19}F NMR spectra as a function of temperature (184.0 to 312.3 K) for the 5 isomers of [Co(TTFA)$_2$(CH$_3$py)$_2$] (**4**) in CD$_2$Cl$_2$, and (iii) Eyring plots of the isomerization rate constants obtained by Kubo–Sack fitting. ([complex]/[free CH$_3$py] = 1:3.5).

Figure 15. Variable pressure ^{19}F NMR spectra of [Co(TTFA)$_2$-(CH$_3$py)$_2$] (**4**) with excess CH$_3$py in CD$_2$Cl$_2$ at 265.5 K.

does not alter the assignment of a ring-opening mechanism for the isomerization processes of [Co(TTFA)$_2$-(CH$_3$py)$_2$] (**4**). Experiments with variable concentrations ([**4**]/[free CH$_3$py]: from 1/0 to 1/8) of the free ligand CH$_3$py were also performed at 264.15 K (Supporting Information, Figure S9). The ^{1}H NMR methyl region for coordinated CH$_3$py and the ^{19}F NMR spectra remain identical: this demonstrates that the kinetic process is intramolecular and not affected by the presence or not of an excess CH$_3$py. A further criterion for the mechanistic assignment is to look at the activation volumes for the isomerization processes. The effect of pressure on the ^{19}F NMR spectrum was studied up to 200 MPa in the slow exchange regime (Supporting Information, Figure S10). Figure 15 shows clearly a line narrowing with pressure, which is indicative of positive activation volumes and confirms the occurrence of a ring-opening (bond breaking)

at the isomerization transition states. The thermodynamic isomerization volumes of the order of 0–2 cm^3 mol^{-1} and the kinetic activation volumes of the order of +10 cm^3 mol^{-1} are given in Table 6.

The complex [Co(TTFA)$_2$(CF$_3$py)$_2$] (**5**) differs from **3** and **4** by the replacement of the monodentate CH$_3$py ligand by the less basic CF$_3$py ligand. The main change in behavior is the strongly increased coordinated/free ligand exchange rate observed for the fluorinated ligand (more than 2 orders of magnitude) and the moderate increase in the rates of the isomerization processes. The temperature dependence of the ^{19}F NMR spectra of the CF$_3$ signal of TTFA has been analyzed with the same exchange matrix as used for compound **4** (Figure 8 and Supporting Information, Table S5). Two typical simulations in the kinetic relevant isomerization domain (267.7 and 273.2 K) are shown in Figure 16. The corresponding thermodynamic and kinetic parameters are reported in Table 6. The rates of the **I ↔ II**, **II ↔ V**, and **II ↔ IV** pathways increase by a factor 4, that of the **III ↔ IV** by a factor 2, while the rate of the **III ↔ V** pathway is unperturbed in **5** compared to **4**. These increases in rate constants are reflected mainly by the increase of the $\Delta S^{\ddagger}$ values, while the $\Delta H^{\ddagger}$ values remain approximately the same.

The intermolecular coordinated/free CF$_3$py exchange rate constants have been obtained by analyzing the temperature behavior the ^{19}F NMR signals of the co-ordinated CF$_3$py ligand (Figure 17), which show an added broadening, compared to the CF$_3$ signals of TTFA. For this purpose the exchange matrix (Supporting Information, Table S5) must be extended by adding, in principle, six exchange rate constants corresponding to the five isomers. To simplify the analysis and to avoid the addition of too many parameters in the simulation, it was assumed that the *trans* effect was the main factor determining the intermolecular exchange rates. With this assumption the number of intermolecular exchange rate constants is reduced to three: k_{cis-F} and k_{cis-S} for the exchange of a pyridine *trans* to a trifluoromethyl or to a thienyl group of TTFA in a *cis* isomer, k_{trans} for a pyridine *trans* to another pyridine in a *trans* isomer. The isomerization and ligand exchange rate constants can be compared in Figure 17 and Table 6. The interaction with cobalt of the TTFA oxygen proximate to the CF$_3$ is the weakest (ease of ring-opening) and explains the slowest exchange rate observed for the *trans* CF$_3$py ligand. On the other hand the absence of this effect in the *trans* isomers explains the faster CF$_3$py exchange rates observed for **III** and **IV**. Notice that the activation parameters for these monodentate ligand exchange processes were obtained in a small temperature range and therefore must be looked

Table 6. Equilibrium Constants, Thermodynamic Parameters, Rate Constants, and Activation Parameters for the Isomerization Reactions Between the Five Isomers of $[Co(TTFA)_2(CH_3py)_2]$ (**4**) (184.0−312.3 K) and $[Co(TTFA)_2(CF_3py)_2]$ (**5**) (198.7−273.2 K) in CD_2Cl_2 ([complex]/[free monodentate ligand] = 1:3.5 and 1:3, respectively)

thermodynamic	IV→I	IV→II	IV→III	IV→V	kinetic	I→II	II→V	III→IV	II→IV	III→V	trans →L	cis-S →L	cis-F →L
					$[Co(TTFA)_2(CH_3py)_2]$								
$K_{IV,j}^{265} \pm 0.05$	0.65	0.98	0.74	0.67	$k^{265} \pm 200^a$	1190	500	2230	560	570			
$\Delta H_{IV,j}^0 \pm 0.2^b$	+5.45	+5.19	−0.53	+1.38	$\Delta H^{\ddagger} \pm 0.6^b$	52.29	54.90	53.21	57.91	52.32			
$\Delta S_{IV,j}^0 \pm 0.7^c$	+16.9	+19.5	−4.5	+1.8	$\Delta S^{\ddagger} \pm 2.3^c$	+12.3	+14.9	+21.0	+27.1	+6.3			
$\Delta V_{IV,j}^0 \pm 1^d$	0.0	+0.4	−1.2	−2.0	$\Delta V^{\ddagger} \pm 1^d$	+7.9	+11.3	+10.2	+11.2	+6.3			
					$[Co(TTFA)_2(CF_3py)_2]$								
$K_{IV,j}^{265} \pm 0.05$	0.30	0.37	0.68	0.24	$k^{265} \pm 150^a$	4430	2020	4070	2280	650	3650	2400	1400
$\Delta H_{IV,j}^0 \pm 0.2^b$	+6.75	+5.16	−0.73	+1.84	$\Delta H^{\ddagger} \pm 0.5^b$	59.93	54.45	53.87	57.70	56.11	60.02	70.06	75.02
$\Delta S_{IV,j}^0 \pm 0.6^c$	+15.4	+11.3	−0.6	−4.9	$\Delta S^{\ddagger} \pm 1.8^c$	+52.0	+24.8	+28.4	+38.1	+21.7	+50.8	+85.1	+99.3

^{a} s^{-1}, ^{b} $kJ\ mol^{-1}$, ^{c} $J\ K^{-1}\ mol^{-1}$ and ^{d} $cm^3\ mol^{-1}$,
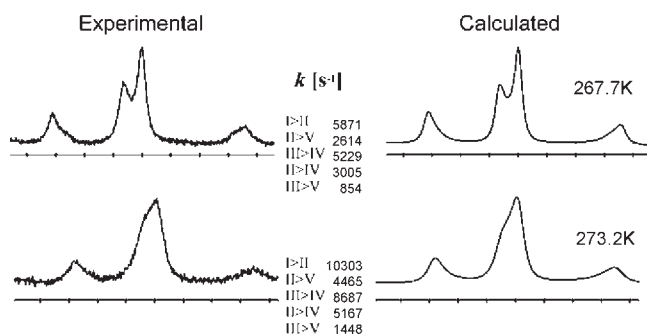
Figure 16. Selection of experimental (left) and Kubo−Sack calculated (right) TTFA ^{19}F NMR spectra of $[Co(TTFA)_2(CF_3py)_2]$ (**5**) in CD_2Cl_2 ([complex]/[free CH_3py] = 1:3).

on with caution. Finally the TTFA ring-opening is still the main operative mechanism for $[Co(TTFA)_2(CF_3py)_2]$ (**5**) despite the relatively fast dissociative CF_3py ligand exchange. This is proven by the dominance of the **III ↔ IV** isomerization pathway which should be absent for a monodentate ligand dissociation activation step. There is also no necessity to introduce the **I ↔ III** pathway to obtain high quality spectral fitting over the whole temperature range which is required for this latter mechanism (see Figure 12). One can, however, not exclude a small contribution of this pathway for compound **5**.

1D saturation transfer and 2D EXSY NMR rate constant and exchange kinetic connectivity experiments have been performed on octahedral diamagnetic Ga(III) *tris*-chelates[7] and paramagnetic V(III) dichloro-*bis*-chelates[9] to complete variable temperature line-broadening NMR isomerization kinetic studies. Similar experiments performed on complexes **4** and **5** confirm the exchange paths determined by variable temperature line-broadening. The 1D saturation transfer (Supporting Information, Figures S12 and S13) and the 2D EXSY (Supporting Information, Figure S14) experiments are limited to the slow exchange domain: this is a serious problem when different exchange paths characterized by fairly different rates are occurring. Further, in this situation, the choice of an optimum mixing time and the unavoidable cross peaks due to two consecutive paths which render uncertain the exchange connectivities are additional difficulties. The small accessible temperature range also limits the accuracy in the determination of the activation parameters.
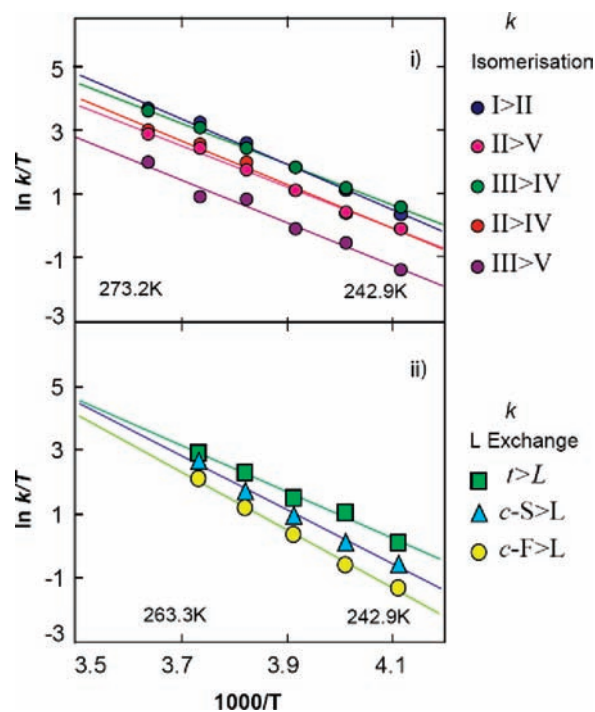
Figure 17. Eyring plots of the isomerization rate constants obtained from the TTFA spectra (i) and coordinated/free ligand exchange rate constants obtained from the bound CF_3py signals (ii) of $[Co(TTFA)_2(CF_3py)_2]$ (**5**) in CD_2Cl_2 ([complex]/[free CH_3py] = 1:3).

4. Discussion

Mechanistically, non bond-rupture twist mechanisms predominate for the racemization and the isomerization reactions of tropolonate, catecholate, and dithiocarbamate metal chelates, whereas intramolecular bond-rupture mechanisms are commonly implicated in acetylacetonate complexes.[2,10,13,15] In this study the structural properties, the rates and the mechanisms of isomerization of the two cobalt(II) six-coordinate *tris*-chelate complexes $[Co(HFA)_2bpic]$ (**1**) and $[Co(TTFA)_2bpy]$ (**2**) differ markedly from those of the three *bis*-chelate complexes $[Co(HFA)_2(CH_3py)_2]$ (**3**), $[Co(TTFA)_2(CH_3py)_2]$ (**4**), and $[Co(TTFA)_2(CF_3py)_2]$ (**5**). What is common to the five complexes is the observation in dichloromethane solution of all possible isomers, from one for **1** up to five for **4** and **5** (Figure 2). All *cis*-N isomers form pairs of enantiomers not distinguishable by NMR, whereas the *trans*-N isomers are achiral. Line broadening NMR shows that the *tris*-chelates

Table 7. Correlations between Complexes' Ground-State Structures, As Determined in the Solid State by X-ray (Figure 3), and the Isomerization Mechanisms

(A) Bite Angle (α) and Normalized Bite (b) Metrics				
	α(OCoO)	α(NCoN)	b(OCoO)	b(NCoN)
Δ- [Co(HFA)$_2$bpic] (**1**)	86.81, 86.57	78.07	1.37	1.26
Δ-I-[Co(TTFA)$_2$bpy] (**2**)	86.05, 85.75	77.59	1.36	1.25
trans-[Co(HFA)$_2$(CH$_3$py)$_2$] (**3**)	88.54		1.40	
Δ-V-[Co(TTFA)$_2$(CH$_3$py)$_2$] (**4**)	88.21	93.0	1.39	1.45
III-[Co(TTFA)$_2$(CF$_3$py)$_2$] (**5**)	89.37		1.41	

(B) Twist Angles (θ) for the Three *cis* Isomers			
pseudo C$_3$ face	twist angle[a]	isomerization	mechanism[b]
	Δ-[Co(HFA)$_2$bpic] (**1**)		
O1O2O3	56.7	Δ-1 $\rightarrow$ Λ-1	Rây−Dutt
O1O3N1	**51.5**	**Δ-1 $\rightarrow$ Λ-1**	**Bailar**
O1N1N2	57.7	Δ-1 $\rightarrow$ Λ-1	Rây−Dutt
O1N2O2	56.9	Δ-1 $\rightarrow$ Λ-1	Rây−Dutt
	Δ-I-[Co(TTFA)$_2$bpy] (**2**)		
O1O2O3	56.8	Δ-I-2 $\rightarrow$ Λ-II-2	Rây−Dutt
O1O3N1	**47.6**	**Δ-I-2 $\rightarrow$ Λ-V-2**	**Bailar**
O1N1N2	56.6	Δ-I-2 $\rightarrow$ Λ-II-2	Rây−Dutt
O1N2O2	54.1	Δ-I-2 $\rightarrow$ Λ-V-2	Rây−Dutt
	[Co(TTFA)$_2$(CH$_3$py)$_2$] (**4**)		
O1O2O2A	58.3	Δ-V-4 $\rightarrow$ Λ-II-4	Rây−Dutt
O1O2AN1	61.6	Δ-V-4 $\rightarrow$ Λ-I-4	Bailar
O1N1N1A	58.3	Δ-V-4 $\rightarrow$ Λ-II-4	Rây−Dutt
O1N1AO2[c]	64.9	Δ-V-4 $\rightarrow$ Λ-I-4	Rây−Dutt
O1N1AO2[c]	55.1	Δ-V-4 $\rightarrow$ IV-4[d]	Rây−Dutt
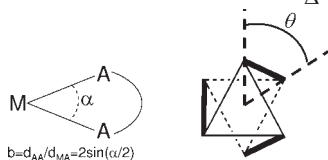
[a] Average of the twist angles of the 3 summits of the non-equilateral triangles. [b] The two mechanisms observed by NMR are indicated in bold. [c] Both clockwise and anticlockwise twists are possible for this face. [d] *cis*/*trans* isomerization.

isomerize according to Bailar twist mechanisms, whereas the *bis*-chelates isomerize 3 orders of magnitude slower by dechelation of one arm of a bidentate ligand forming TBP five coordinate intermediates.

Structure/isomerization mechanism/rate relationships have been suggested from the results of NMR investigations[10] and theoretical simulations[13,15] for the racemization of chiral *tris*-chelates of the M^{III}L$_3$ (L = A-A, A-B) type. Kepert[44] has already parametrized some of these relationships in the 1970s for metal ions in which electronic considerations, such as ligand-field stabilization energy do not play a significant role. An obvious choice for the twist isomerization reactions coordinate is the twist angle θ (Table 7). It amounts to 60° for a perfectly octahedral geometry and 0° for a perfectly prismatic one. One expects that a twist according to a Bailar mechanism (rotation around the C$_3$ axis) or to a Rây−Dutt mechanism (rotation around one of the other three C$_3$ axis of the octahedron defined by the complex's donor atoms which is not a C$_3$ axis of the complex) will be energetically favored for a compound with a structure substantially distorted from the perfectly octahedral geometry of the donor atoms toward a prismatic geometry, with a twist angle significantly lower than 60° (Figure 1). A correlation between complexes'

ground-state structures, as determined in the solid state by X-ray, and isomerization rates have been found, demonstrating that less twisted (small θ) structures isomerize faster.[45,46] Kepert has shown that the twist angle θ is related to the bite angle α or better to the normalized bite b values (Table 7). Complexes with larger bite b values, larger chelates and/or shorter metal−ligand bonds, tend to have larger twist angles θ and slower rates of isomerization.[44] Theory also predicts that the Bailar twist mechanism has a lower activation barrier relative to the Rây−Dutt mechanism as b decreases across a series of metal−ligand complexes.[7,12,44] Different values for b as cutoff when the Bailar twist becomes the predominant intramolecular rearrangement mechanism are reported, ranging from 1.3 to 1.5.

Compared to the widely studied symmetric ML$_3$ type of complexes, structure/isomerization mechanism/rate relationships for compounds **1** to **5** are less obvious to establish because of the lower symmetry of these Co(II) complexes which have 4 oxygen donor atoms (2 symmetric or asymmetric acetylacetonates) and 2 nitrogen donor atoms (1 bipyridine or 2 pyridines). For compound Δ-**1** and Δ-I-**2** (Table 7) the average bite angle α and the normalized bite

(44) Kepert, D. L. *Prog. Inorg. Chem.* **1977**, *23*, 1−65.

(45) Horrocks, W. D.; Hall, D. W. *Inorg. Chem.* **1971**, *10*, 2368−2370.
(46) Eaton, S. S.; Eaton, G. R. *J. Am. Chem. Soc.* **1973**, *95*, 1825−1829.

b values for the acetylacetonates (86.3°, 1.36/1.37) are within the mechanism cutoff range, whereas the values for the bipyridines (77.8°, 1.25/1.26) are indicative of a Bailar twist mechanism. For the $\Delta \leftrightarrow \Lambda$ enantiomerization of these 2 *tris*-chelates one can calculate 4 twist angles corresponding to the rotation around the 4 pseudo C_3 axes (passing through the geometric barycenter of two opposing triangles of the donor atoms octahedron). Interestingly, the twist angle for the Bailar twist (51.5° for Δ-**1**, 47.6° for Δ-I-**2**) is clearly smaller than for the three possible Rây—Dutt twists (56.7°—57.7°, 54.1°—56.8°, respectively) in conformity with the mechanism determined by NMR line-broadening in CD_2Cl_2 solution. The rates of the Bailar twist enantiomerization of Δ-**1** and Δ-I-**2** are of the same order of magnitude. Δ-I-**2** reacts 2 times faster than Δ-**1** at 190 K, and 3 times slower at 265 K. The difference in the temperature behavior of the rate constants of these two compounds is due to smaller enthalpies and entropies of activation for Δ-I-**2** (Table 3). A fast optical inversion has already been reported by La Mar[16] for [Co(acetylacetonate)$_2$(4,7-dimethyl-1,10-phenantroline)] in CHCl$_3$. Its rate $k/10^6$ s^{-1} is intermediate at 298 K to those of the two *tris*-chelates studied: 3.6 (**1**) < 5 ([Co(acac)$_2$(dimethyl-phenantroline)]) < 10.1 (I-**2**). By analogy we can now also assign a Bailar twist mechanism for this Co(II) *tris*-chelate studied earlier. For compound **2** the rate for the I-**2**↔V-**2** Bailar twist isomerization, accompanied by optical inversion, is 4 (190 K) to 2 (265 K) times slower than the enantiomerization rate of the I-**2** isomer.

The crystal structures of the three *bis*-acetylacetonate-*bis*-pyridine Co(II) complexes, **3** to **5**, exhibit a nearly octahedral arrangement of the six donor atoms (Figure 3 and Table 2). The bite angles α (88.54°, 88.21°, 89.37°, respectively) and the normalized bites *b* (1.40, 1.39, 1.41) values for the acetylacetonate ligands are now clearly larger than in compound **1** and I-**2**, and this is especially true for the 2 monodentate pyridines (α = 93° and *b* = 1.45) which are no longer linked as in the bidentate bpic and bpy ligands (Table 7). These larger values disfavor the twist mechanisms. This prediction is even more perceptible from the crystallographic twist angle θ values of the Δ-V-**4** complex, ranging from 55.1° to 64.9°, which are close to the 60° value for a perfectly octahedral geometry. The energy for a twist isomerization becomes therefore too high, and compounds **3** to **5** isomerize preferably by dechelation of one arm of an acetylacetonate ligand as shown by the NMR line-broadening experiments.

A schematic representation of the isomer populations, the exchanges paths, and the frequency of exchange events for the three *bis*-bidentate complexes **3**, **4**, and **5** at 265 K is drawn in Figure 18. These complexes exist in the form of chiral *cis* and achiral *trans* isomers. The percentage of the *trans* isomers increases from **3** to **5**, from 30, to 43, up to 65%. This increase is correlated with the introduction of ligands with weaker donor groups, the replacement of HFA by TTFA, followed by the replacement of CH$_3$py by CF$_3$py. For the three compounds the *trans* isomers populations decrease with increasing temperature. This is the inverse of what would be the expected behavior of a symmetric molecule with the parallel decrease from 15 at 190 K to 10 at 265 K of the dielectric constant ε of the solvent CD$_2$Cl$_2$ with increasing temperature.[47] The isomerization reaction volumes $\Delta V°$ for

(47) Morgan, S. O.; Lowry, H. H. *J. Phys. Chem.* **1930**, *34*, 2385–2432.
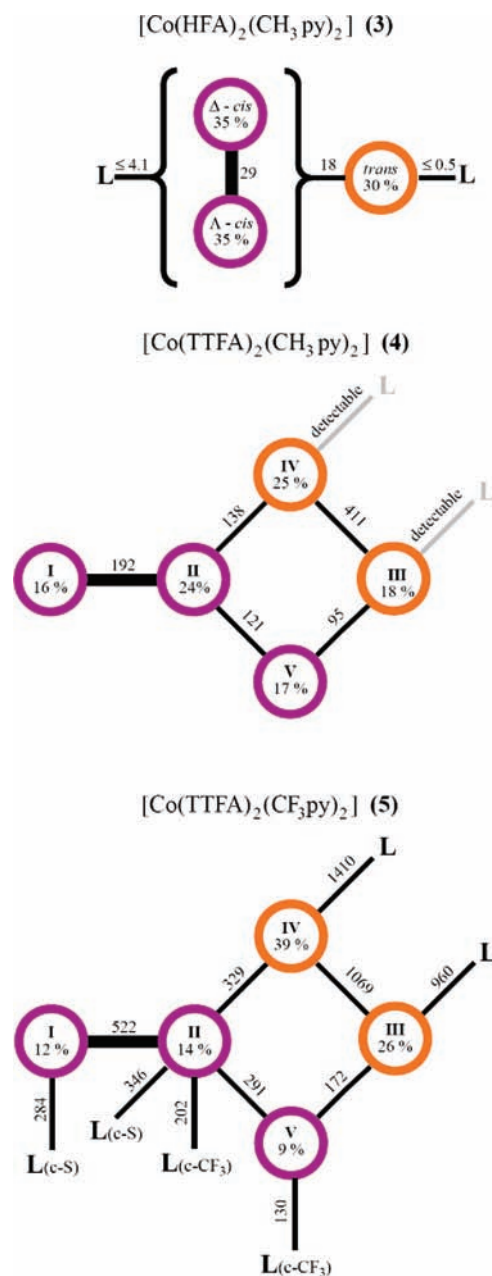
Figure 18. Schematic representation of the isomer populations, exchange paths, and frequency of exchange events (s^{-1}) for the isomerizations of the three *bis*-bidentate Co(II) complexes **3**, **4**, and **5**, at 265 K in CD$_2$Cl$_2$. Two intermediates are possible for the Δ-*cis* ↔ Λ-*cis* path of **3** and for the **I** ↔ **II** path of **4** and **5** (Supporting Information, Table S5).

compounds **3** and **4** are very small, with absolute values within the 0.0 and +2.4 cm^3 mol^{-1} range. These small values are indicative of very similar partial molar volumes and of similar electrostriction effects on the different isomers. On the contrary, the activation volumes $\Delta V^{\ddagger}$ for the isomerization reactions are clearly positive for **3** (+ 2.4 to +6.2 cm^3 mol^{-1}) and **4** (+ 6.3 to +11.2 cm^3 mol^{-1}) confirming the bidentate HFA and TTFA ring-opening as the rate determining step. The less accurately determined activation entropies $\Delta S^{\ddagger}$ (positive except one) also support this assignment: **3** (−11.8 to + 45.9 J K^{-1} mol^{-1}), **4** (+ 6.3 to + 27.1 J K^{-1} mol^{-1}), **5** (+ 21.7 to + 38.1 J K^{-1} mol^{-1}).

In Figure 18, the frequency of exchange events is the product of the first order rate constant $k_{i>j}$ (reaction from

isomer, or enantiomer, *i* to *j*) by the mole fraction P_i. This frequency is the same for the forward and backward reaction, and allows a direct comparison of the frequency of the events which are rate constants balanced by the populations. If the energies of the intermediates would be equal, then the frequency of events should be proportional to the number of intermediates for a given pathway. This behavior is observed for compound **3**, where the Δ-*cis* $\leftrightarrow$ Λ-*cis* enantiomerization frequency is almost twice the *cis* $\leftrightarrow$ *trans* isomerization frequency. For compounds **4** and **5**, the same argument predicts that the frequency of the **I** $\leftrightarrow$ **II** isomerization path is twice as large as the frequencies of the other isomerization paths. This is observed, with ratios of 1.4 to 2.0 for **4** and 1.6 to 3.0 for **5**. The only exception, observed for both compounds, is larger isomerization frequencies for the **III** $\leftrightarrow$ **IV** isomerization path between the two *trans* isomers which are 2.0 times faster than the **I** $\leftrightarrow$ **II** isomerization paths. For compound **4**, the rate of coordinated/ free CH_3py intermolecular ligand exchange is hardly detectable and too small to be measured by NMR: one can therefore exclude a mechanism involving the dissociation of the monodentate ligand at the transition state. A small contribution of this mechanism for compound **5** cannot be excluded.

5. Conclusion

In conclusion, a solid state structure/isomerization mechanism/rate correlation has been established for Co(II) *tris*- and *bis*-chelates. The two *tris*-chelate complexes [Co(HFA)₂bpic] (**1**) and [Co(TTFA)₂bpy] (I-**2**), with a distorted octahedral solid state structure, show one and three isomers in dichloromethane solution and isomerize/tautomerize very rapidly according to Bailar twist mechanisms. The three *bis*-chelate complexes [Co(HFA)₂(CH₃py)₂] (*trans*-**3**), [Co(TTFA)₂-(CH₃py)₂] (V-**4**), and [Co(TTFA)₂(CF₃py)₂] (II-**5**), with a close to octahedral symmetry in the solid state, show all possible isomers in solution (two, five, and five). They isomerize/tautomerize 3 orders of magnitude slower as the *tris*-chelates, by an intramolecular dissociative mechanism involving a ring-opening of an arm of a bidentate ligand to form a TBP intermediate with a dangling bidentate ligand. In other words, the replacement of a bidentate N donor molecule by two independent N donor molecules reduces dramatically the rates of isomerization/tautomerization, and inhibits the Bailar twist in favor of a dissociative intramolecular mechanism.

Supporting Information Available: Variable temperature and variable pressure NMR data; crystallographic information files (CIF). This material is available free of charge via the Internet at http://pubs.acs.org.